JOURNAL OF GEOPHYSICAL RESEARCH, VOL. 108, NO. D16, 8543, doi:10.1029/2002JD002891, 2003

International Photolysis Frequency Measurement and Model Intercomparison (IPMMI): Spectral actinic solar flux measurements and modeling

A. F. Bais,[1] S. Madronich,[2] J. Crawford,[3] S. R. Hall,[2] B. Mayer,[2,4] M. van Weele,[5] J. Lenoble,[6,7] J. G. Calvert,[2] C. A. Cantrell,[2] R. E. Shetter,[2] A. Hofzumahaus,[8] P. Koepke,[9] P. S. Monks,[10] G. Frost,[11] R. McKenzie,[12] N. Krotkov,[13] A. Kylling,[14] W. H. Swartz,[15] S. Lloyd,[15] G. Pfister,[16,17] T. J. Martin,[18,19] E.-P. Roeth,[8] E. Griffioen,[20,21] A. Ruggaber,[22] M. Krol,[23] A. Kraus,[24,25] G. D. Edwards,[10,17] M. Mueller,[18,26] B. L. Lefer,[2] P. Johnston,[12] H. Schwander,[22] D. Flittner,[27] B. G. Gardiner,[28] J. Barrick,[3] and R. Schmitt[29]

Received 29 August 2002; revised 5 February 2003; accepted 26 February 2003; published 17 July 2003.

[1] The International Photolysis Frequency Measurement and Model Intercomparison (IPMMI) took place in Boulder, Colorado, from 15 to 19 June 1998, aiming to investigate the level of accuracy of photolysis frequency and spectral downwelling actinic flux measurements and to explore the ability of radiative transfer models to reproduce the measurements. During this period, 2 days were selected to compare model calculations with measurements, one cloud-free and one cloudy. A series of ancillary measurements were also performed and provided parameters required as input to the models. Both measurements and modeling were blind, in the sense that no exchanges of data or calculations were allowed among the participants, and the results were objectively analyzed and compared by two independent referees. The objective of this paper is, first, to present the results of comparisons made between measured and modeled downwelling actinic flux and irradiance spectra and, second, to investigate the reasons for which some of the models or measurements deviate from the others. For clear skies the relative agreement between the 16 models depends strongly on solar zenith angle (SZA) and wavelength as well as on the input parameters used, like the extraterrestrial (ET) solar flux and the absorption cross sections. The majority of the models (11) agreed to within about ±6% for solar zenith angles smaller than ~60°. The agreement among the measured spectra depends on the optical characteristics of the instruments (e.g., slit function, stray light rejection, and sensitivity). After transforming the measurements to a common

[1]Laboratory of Atmospheric Physics, Aristotle University of Thessaloniki, Thessaloniki, Greece.
[2]Atmospheric Chemistry Division, National Center for Atmospheric Research, Boulder, Colorado, USA.
[3]NASA Langley Research Center, Hampton, Virginia, USA.
[4]Now at Deutsches Zentrum für Luft-und Raumfahrt, Oberpfaffenhofen, Germany.
[5]Royal Netherlands Meteorological Institute, De Bilt, Netherlands.
[6]Equipe Interactions Rayonnement Solaire Atmosphere, Universite Joseph Fourier, Grenoble, France.
[7]Also at Laboratoire d' Optique Atmosphérique/Université des Sciences et Technologies de Lille, Lille, France.
[8]Institut für Chemie und Dynamik der Geosphaere II: Troposphaere, Forschungszentrum Juelich, Juelich, Germany.
[9]Meteorological Institute, University of Munich, Munich, Germany.
[10]Department of Chemistry, University of Leicester, Leicester, UK.
[11]Aeronomy Laboratory, National Oceanic and Atmospheric Administration, Boulder, Colorado, USA.
[12]National Institute of Water and Atmospheric Research, Lauder, New Zealand.
[13]Goddard Earth Sciences and Technology Center, University of Maryland at Baltimore County, Baltimore, Maryland, USA.
[14]Norwegian Institute for Air Research, Kjeller, Norway.
[15]Applied Physics Laboratory, Johns Hopkins University, Laurel, Maryland, USA.
[16]Institute for Geophysics, Astrophysics and Meteorology, Karl-Franzens University, Graz, Austria.
[17]Now at Atmospheric Chemistry Division, National Center for Atmospheric Research, Boulder, Colorado, USA.
[18]Fraunhofer Institute for Atmospheric Environmental Research, Garmisch-Partenkirchen, Germany.
[19]Now at Karl-Franzens University, Graz, Austria.
[20]Department of Earth and Atmospheric Sciences, York University, North York, Ontario, Canada.
[21]Now at Hamilton Regional Cancer Centre, Hamilton, Ontario, Canada.
[22]Meteorological Institute, University of Munich, Munich, Germany.
[23]Institute for Marine and Atmospheric Research, Utrecht, Netherlands.
[24]Institut für Atmosphaerische Chemie, Forschungszentrum Juelich GmbH, Juelich, Germany.
[25]Now at Research and Development Grünenthal GmbH, Aachen, Germany.
[26]Now at Dresdener Bank AG, Frankfurt, Germany.
[27]Institute of Atmospheric Physics, University of Arizona, Tucson, Arizona, USA.
[28]British Antarctic Survey, Cambridge, UK.
[29]Meteorologie Consult GmbH, Glashütten, Germany.

0148-0227/03/2002JD002891

spectral resolution, two of the three participating spectroradiometers agree to within ~10% for wavelengths longer than 310 nm and at all solar zenith angles, while their differences increase when moving to shorter wavelengths. Most models agree well with the measurements (both downwelling actinic flux and global irradiance), especially at local noon, where the agreement is within a few percent. A few models exhibit significant deviations with respect either to wavelength or to solar zenith angle. Models that use the Atmospheric Laboratory for Applications and Science 3 (ATLAS-3) solar flux agree better with the measured spectra, suggesting that ATLAS-3 is probably more appropriate for radiative transfer modeling in the ultraviolet. *INDEX TERMS:* 0365 Atmospheric Composition and Structure: Troposphere—composition and chemistry; 0394 Atmospheric Composition and Structure: Instruments and techniques; 3359 Meteorology and Atmospheric Dynamics: Radiative processes; 3367 Meteorology and Atmospheric Dynamics: Theoretical modeling; *KEYWORDS:* actinic flux, solar ultraviolet radiation, UV modeling, UV spectral measurements, model intercomparison

Citation: Bais, A. F., et al., International Photolysis Frequency Measurement and Model Intercomparison (IPMMI): Spectral actinic solar flux measurements and modeling, *J. Geophys. Res.*, *108*(D16), 8543, doi:10.1029/2002JD002891, 2003.

1. Introduction

[2] Atmospheric chemistry in the lower atmosphere depends strongly on photoreactions, which are driven by solar radiation, especially in the ultraviolet and visible spectral regions. In such processes the targets are particles or molecules susceptible to radiation from all directions, rather than horizontal surfaces intercepting radiation fluxes in proportion to the cosine of the angle of incidence. The radiation quantity that best describes the geometry in these photoreactions is the actinic (4π sr) flux, F, which can be written as:

$$F = \int_0^{2\pi} \int_{-\pi/2}^{\pi/2} L(\varphi,\theta) \sin\theta d\theta d\varphi + F_b, \qquad (1)$$

where $L(\varphi,\theta)$ is the diffuse radiance in the direction (φ,θ), φ being the azimuthal angle and θ the zenith angle, and F_b is the actinic flux received from the direction of the Sun and equals the direct irradiance, E_b, received on a plane perpendicular to the direction of the beam.

[3] The actinic flux comprises the same photons that are recorded by global irradiance, E; the actinic flux is simply a radiation quantity of different geometry. The same processes therefore govern its spatial and temporal variability when considering its interaction with the atmosphere. However, with respect to geometry, significant differences can be encountered, especially in connection to the effect of solar zenith angle (SZA) variations. One of the most important differences is the contribution of the direct irradiance, which for global irradiance (downwelling diffuse plus direct irradiance received on a horizontal plane) is weighted with the cosine of the solar zenith angle, θ_o, while for actinic flux, no weighting takes place. The global irradiance, E, is defined as:

$$E = \int_0^{2\pi} \int_{-\pi/2}^{\pi/2} L(\varphi,\theta) \cos\theta \sin\theta d\theta d\varphi + E_b(\cos\theta_o). \qquad (2)$$

[4] From equation (1) it is clear that diffuse radiation from any direction contributes equally to actinic flux, since the radiance $L(\varphi,\theta)$ is not weighted with the $\cos\theta$ as in equation (2). Thus diffuse radiation close to the horizon, which is considered negligible when dealing with irradiance, is of equal importance to radiation arriving from other directions; for example, from the zenith. This introduces difficulties when comparing measurements and model estimates of actinic flux at locations with an imperfect field of view since the presence of even short obstacles may significantly affect the measurement, leading either to reduction (by blocking part of the diffuse radiation) or to an increase (through direct reflections) of the signal. The distance to the obstructions is also important and can introduce wavelength-dependent effects. Because the shorter wavelengths are absorbed and scattered more efficiently, only radiation from short distances contributes to the actinic flux at these wavelengths, and hence distant obstacles affect only the longer wavelengths.

[5] The ultraviolet and visible actinic flux at a given position within the atmosphere is determined by the absorption and scattering of the incoming solar radiation by the atmospheric constituents and depends strongly on the path length traversed by the radiation. Thus actinic fluxes near the surface are expected to respond to changes in atmospheric composition which, in the absence of clouds, refers mainly to ozone, SO_2, NO_2, and aerosols. Clouds play a very important and complicated role, mainly leading to a reduction of actinic flux, although under certain circumstances, increases may occur. The vertical distribution of those atmospheric constituents also affects the actinic flux through the modification of absorption and scattering at various altitudes from the ground. Finally, the surface albedo is of significant importance, having a direct influence on the actinic flux (upwelling component) while in global irradiance it acts only indirectly through multiple scattering.

[6] In response to stratospheric ozone depletion, the scientific and technological challenges associated with both the measurement and modeling of solar ultraviolet radiation have received considerable attention in the past decade. Most of the attention concerning measurements was focused on the spectral irradiance incident on a horizontal surface rather than on the actinic flux. Only in the late 1990s did a few groups start developing spectroradiometers capable of recording actinic flux spectra in the ultraviolet and visible regions [*Hofzumahaus et al.*, 1999; *Shetter and Mueller*, 1999; *Mueller et al.*, 1995; *Kraus and Hofzumahaus*, 1998]. On the other hand, radiative transfer (RT) models capable of

Table 1. List of the Acronyms Used to Identify the Models Participated at IPMMI and the Corresponding Institutes

IPMMI ID	Model Name	Institute
ACD	TUV 4.0	Atmospheric Chemistry Division, National Center for Atmospheric Research
AES	JMAM	York University, Department of Earth and Atmospheric Sciences
BAS	BASRTM	British Antarctic Survey, Cambridge
BM1	LibRadtran	Atmospheric Chemistry Division, National Center for Atmospheric Research
BM2	LibRadtran	Atmospheric Chemistry Division, National Center for Atmospheric Research
BM3	LibRadtran	Atmospheric Chemistry Division, National Center for Atmospheric Research
JHU	JHU/APL	The Johns Hopkins University Applied Physics Laboratory
KFA	ART	Institut fuer Chemie und Dynamik der Geosphaere II: Troposphaere Forschungszentrum Juelich
KFU	TUV 3.9	Institute for Geophysics, Astrophysics and Meteorology, Karl-Franzens University, Graz
KNM	DAK	Royal Netherlands Meteorological Institute
LOA	USTL-SOS	LOA/USTL, Lille
MAR		Institute for Marine and Atmospheric Research, Utrecht
NIL	LibRadtran	Norwegian Institute for Air Research
NOA	TUV 3.8	Aeronomy Laboratory, National Oceanic and Atmospheric Administration
OPT	TOMRAD	Goddard Earth Sciences and Technology Center, University of Maryland at Baltimore County
UMU	STAR	Meteorological Institute, University of Munich

calculating actinic fluxes had been developed well before the 1990s, despite the lack of reliable measurements for their validation. In atmospheric chemistry the main use of actinic fluxes is the determination of photolysis frequencies (j) for various photoreactions occurring in the atmosphere. While from its definition the actinic flux refers to 4π sr geometry, for technical reasons, most of the existing instruments are designed to measure the actinic flux from only one hemisphere (2π sr), either the upper (downwelling flux) or the lower (upwelling flux). The 4π sr actinic flux can be derived, then, by combining two independent measurements. The 4π sr actinic flux is meaningful only if measurements are made some distance above the ground. When the instrument is at ground level, most of the radiation comes from the upper hemisphere, unless the surface albedo is high.

[7] Recently, considerable effort has been spent upon the quality control of the actinic flux and photolysis frequency measurements and the validation of the relevant RT models. These topics were within the scope of the International Photolysis Frequency Measurement and Model Intercomparison (IPMMI), which took place in Boulder, Colorado, between 15 and 19 June 1998. A detailed measurement program was instituted, which included spectroradiometric measurements of the downwelling (2π sr) actinic flux and irradiance, photolysis frequency measurements for O_3 to $O(^1D)$ and for NO_2 to $O(^3P)$, and various ancillary measurements that were used by the RT models. This paper is one of a series of papers relevant to IPMMI [e.g., *Cantrell et al.*, 2003; *Shetter et al.*, 2003; *Crawford et al.*, 2003; *Edwards and Monks*, 2003] and focuses on spectrally resolved actinic fluxes. It presents a detailed comparison between model- and measurement-derived spectra of 2π sr fluxes and irradiance during the campaign and attempts to quantify and investigate the differences observed both among different models (section 3) and measuring systems (section 4) and also between models and measurements (section 5).

2. Modeling and Measurement of Spectral Solar Fluxes at the Surface

2.1. Radiative Transfer Models

[8] Several radiative transfer models were used in the framework of IPMMI to provide estimates of the spectra of the downwelling (2π sr) component of solar actinic fluxes at the surface for the dates of the measurement campaign. In total, 14 different groups (see Table 1) produced 16 sets of model calculations, since one group provided results from three different models (BM1, BM2, and BM3, together referred to hereinafter as BMx). Some of the groups worked with the same basic RT codes, but because they used different combinations of molecular data, solar flux spectra, and atmospheric structure and composition models, their results were considered in the analysis independently. In fact, such cases provide the opportunity to assess the influence of the users on the results produced by the same model. In addition to the 2π sr flux the model users were asked to provide separately calculated spectra of 4π sr actinic flux, of irradiance on a horizontal surface, and of direct irradiance on a plane normal to the beam. These additional radiometric quantities were required as supplementary information in the assessment of the models' overall performance. The spectra of all four quantities were supposed to cover the spectral range from 280.5 to 699.5 nm in steps of 1 nm and band pass of 1 nm (with unity responsivity), which would be equivalent to a 1-nm-wide rectangular slit function in spectral measurements.

[9] The main objective of the modeling exercise was to assess, both independently and in comparison with spectroradiometric data, how well each model could describe the radiation field in a set of real cases, for which many of the important parameters required as input to the models were available from measurements. For those parameters which could not be retrieved from measurements during the experimental campaign, such as the absorption and scattering cross sections and the extraterrestrial (ET) solar spectrum (including its modification due to the variation of the Sun-Earth distance), the groups were allowed to select what they considered to be the most appropriate source. In other words, they used the parameters that they would use in a study where results only from their own model would be included. The most important of these parameters, as reported by the operators of each model, are listed in Table 2.

[10] Besides the site information (latitude, longitude, and altitude) and the time the parameters provided to the model operators included the vertical distribution of ozone (up to the balloon burst altitude), temperature and pressure vertical profiles (derived from soundings), the ozone column, and the daily course of surface temperature and pressure. How the

Table 2. List of the User-Selected Parameters Used in the Model Calculations

IPMMI ID	Model Name	RT Algorithm	Solar Spectrum, λ nm	Aerosol Profile	O_3 Cross Sections	NO_2 Cross Sections
ACD[a]	TUV 4.0	pseudospherical (four streams)	λ < 400 ATLAS-3; λ > 400 *Neckel and Labs* [1984]	Aerosols between 1.8 and 2.8 km	λ < 350 nm *Molina and Molina* [1986]; λ >350 nm *World Meteorological Organization (WMO)* [1985]	JPL, 1994[b]
AES[a]	JMAM	pseudospherical matrix operator doubling and adding (10 streams)	*WMO* [1985]	constant concentration 1.6–3.0 km, adjusted to AOD	λ < 325 nm *Molina and Molina* [1986]; λ > 325 nm GOME	JPL, 1997[b]
BAS	BASRTM	pseudospherical DISORT (16 streams)	λ < 420 ATLAS-2 (shift for air); λ > 419.9 *Arvesen et al.* [1969]	*Shettle and Fenn* [1979] (continental/rural)	*Malicet et al.* [1995]	JPL, 1997[b]
BM1[a]	LibRadtran	Monte Carlo	λ < 407.8 ATLAS-3; 407.8 < λ < 419.9 ATLAS-2; λ > 419.9 Modtran 3.5	*Shettle* [1989] (volcanic background, rural, spring-summer)	*Molina and Molina* [1986]	*Schneider et al.* [1987]
BM2[a]	LibRadtran	pseudospherical DISORT	λ < 407.8 ATLAS-3; 407.8 < λ < 419.9 ATLAS-2; λ > 419.9 Modtran 3.5	*Shettle* [1989] (volcanic background, rural, spring-summer)	*Molina and Molina* [1986]	*Schneider et al.* [1987]
BM3[a]	LibRadtran	DISORT	λ < 407.8 ATLAS-3; 407.8 < λ < 419.9 ATLAS-2; λ > 419.9 Modtran 3.5	*Shettle* [1989] (volcanic background, rural, spring-summer)	*Molina and Molina* [1986]	*Schneider et al.* [1987]
JHU	JHU/APL	integral equation solution with isotropic scattering	Modtran 3	Modtran 3 rural and tropospheric aerosols, scaled to observations	λ < 350 nm *Molina and Molina* [1986]; λ > 350 nm *WMO* [1985]	JPL, 1997[b]
KFA	ART	pseudospherical with 11 beams	*WMO* [1985]	standard radiation atmosphere (WCP-112, WMO/TD-24, March 1986)	*WMO* [1985]	*Schneider et al.* [1987]
KFU	TUV 3.9	pseudospherical DISORT	λ < 350 SUSIM SL2; λ > 350 *Neckel and Labs* [1984]	*Elterman* [1968] profile	λ > 340 *Bass and Paur* [1985]; λ < 340 *WMO* [1985]	JPL, 1994[b]
KNM[a]	DAK	doubling: adding RT in plane parallel atmosphere	λ < 400 ATLAS-3; λ > 400 *Neckel and Labs* [1984]	1.8–12 km constant number density; 12–30 km very low stratospheric background	*Bass and Paur* [1985]	JPL, 1994[b]
LOA[a]	USTL-SOS	pseudospherical; successive orders of scattering	ATLAS-3	Standard radiation atmosphere (WCP-112, WMO/TD-No 24, March 1986) adjusted to ground altitude and AOD	*Bass and Paur* [1985]	not available
MAR		parametric	SUSIM; *Neckel and Labs* [1984]	no aerosols	λ < 350 nm *Molina and Molina* [1986]; λ > 350 nm *WMO* [1985]	JPL, 1994[b]
NIL[a]	LibRadtran	pseudospherical DISORT (six streams)	λ < 407.8 ATLAS-3; 407.8 < λ < 419.9 ATLAS-2; λ > 419.9 Modtran 3.5	*Shettle* [1989] (volcanic background, rural, spring-summer)	*Bass and Paur* [1985]	JPL, 1997[b]
NOA	TUV 3.8	pseudospherical (eight streams)	λ < 350 SUSIM hi-res; λ > 350 *Neckel and Labs* [1984]	*Elterman* [1968]	λ < 350 nm *Molina and Molina* [1986]; λ > 350 nm *WMO* [1985]	JPL, 1997[b]
OPT	TOMRAD	successive iteration of auxiliary equation of RT; sphericity correction for primary scattering	λ < 407.8 ATLAS-3; 407.8 < λ < 419.9 ATLAS-2; λ > 419.9 Modtran 3.5	aerosol correction, based on IPMMI prescribed aerosol parameters	*Bass and Paur* [1985]	not available
UMU	STAR	pseudospherical (six streams); matrix-operator-model, discrete ordinate, and adding method	λ < 400 ATLAS-3; λ > 400 *Neckel and Labs* [1984]	OPAC, *Hess et al.* [1998]a	GOME; *Burrows et al.* [1999]	*Schneider et al.* [1987]

[a]Model from which the comparison reference is formed.
[b]NO_2 cross sections from JPL, 1994 and JPL, 1997 are identical.

variation of the surface temperature was taken into account was an independent decision of the modelers. Constant values for the aerosol optical depth (AOD) at 550 nm, the single scattering albedo (SSA), the asymmetry parameter (g), and the Angstrom coefficient (a) derived from measurements were also provided. For the surface albedo it was suggested to use the value of 0.03 in the ultraviolet region, which was derived from sporadic measurements with a broadband UV detector, while for wavelengths longer than 420 nm the suggested value was 0.10. The model operators were free to decide how to treat the wavelength dependence of the surface albedo. Some used the suggested constant values for each region (below and above 420 nm), while others decided to vary the albedo linearly in order to avoid distinct changes in their calculations at 420 nm. A more detailed description of the input data and the methods used to derive them are discussed by *Cantrell et al.* [2003]. Two days were chosen for the model calculations, one with clear skies (19 June 1998) and the other with partly cloudy conditions (15 June 1998). Because of the added complexity of dealing with radiative transfer under cloudy conditions, the modelers were asked to provide estimates only on photolysis frequencies under such conditions. Because of the large amount of information, in this paper only spectrally resolved data and calculations under clear skies are analyzed and compared.

[11] On 19 June 1998 the optical depth of the aerosols was very low (on the order of 0.03 ± 0.02 at 550 nm during the morning), and hence a time-independent value of 0.03 was specified for the model calculations. The chosen values for SSA = 0.5, g = 0.45, and a = 1.7 (all at 550 nm) were determined from a nephelometer and a particle/soot absorption photometer, which were sampling air at 5 m above the ground. These measurements are not representative of the aerosols aloft, but they were the only information available for the aerosol properties and thus the only specifications formally provided to the modelers. Even under such low AOD conditions this low value for the SSA can have a significant impact on the actinic fluxes at short wavelengths. In comparison with using SSA = 0.99 the choice of using SSA = 0.5 leads to decreases of actinic fluxes in the ultraviolet of between 6 and 10%, depending on SZA. A recent reevaluation of the nephelometer measurements showed that the initially provided SSA measurement was underestimated and the revised value is 0.62. Separate model calculations showed that for the given AOD, changing the SSA from 0.5 to 0.62 results in a <2% change in the UV actinic flux at the surface. Similar conclusions were drawn for the asymmetry parameter, g. The Angstrom coefficient, however, can have a significant impact on the inferred AOD at shorter wavelengths, as discussed below.

[12] After the distribution of the model intercomparison results among the IPMMI participants some of the groups discovered errors in their original calculations and submitted revised products. In a few cases the errors were due to misinterpretation of the campaign protocol; for example, in the direct irradiance spectra of KFU and NOA, which were given as irradiance incident on a horizontal plane instead of a plane normal to the beam. However, in other cases (JHU, OPT, UMU), more important errors were discovered, which are discussed by the corresponding model operators in section 2.1.2. For those five groups the revised calculations were used in the analysis presented hereinafter.

[13] From Table 2 it can be seen that there are remaining differences in some of the model input parameters, such as the ozone absorption cross sections and the ET spectra. It is expected that these will produce systematic differences. In other model intercomparison studies [e.g., *van Weele et al.*, 2000], such parameters were predefined in order to isolate and uncover conceptual differences among the models, but this was not the aim of IPMMI. With regard to the absorption cross sections of ozone, eight models used those by *Molina and Molina* [1986] and five models used those by *Bass and Paur* [1985], while the remaining three models used cross sections from other sources. The majority of the modelers (nine) preferred to use the Atmospheric Laboratory for Applications and Science 3 (ATLAS-3) ET spectrum, which is one of the most recent and most widely accepted. The remaining seven models used solar spectra from other space missions, introducing systematic differences in their calculations of at least a few percent. In particular, the Modtran 3 ET spectrum (used in the JHU model) differs from ATLAS-3 in the wavelength band 300–315 nm by more than 5% with excursions of up to 20% at single wavelengths.

[14] Differences in the vertical profiles of atmospheric constituents considered by the various models might be another source of differences in their results, but these are not expected to be very important in the IPMMI case. The ozone profile was provided at least up to the balloon burst altitude, and the remaining part could be easily determined by the use of the ozone column that was also given. The aerosol profile was unknown, but due to the very low total optical depth of the aerosols, differences in the profiles assumed in each model are not expected to produce significant differences in the calculated fluxes.

[15] An important aspect of the models that can cause large differences is the treatment of the geometry of the atmosphere in the RT calculations. Many models used the pseudospherical approximations to handle the effect of the curvature of the atmosphere, while others consider the atmosphere structured from plane parallel layers. In the pseudospherical method the sphericity of the Earth's atmosphere is included to calculate the attenuation of the direct beam and the primary scattering, while higher-order (multiple) scattering is calculated in a plane parallel atmosphere [*DeLuisi and Mateer*, 1971; *Dahlback and Stamnes*, 1991]. The differences between these two approaches are expected to be most pronounced at large solar zenith angles. The pseudospherical method is in principle more accurate than the pure plane parallel representation but may also suffer from inaccuracies at large solar zenith angles owing to the approximate treatment of multiple scattering.

2.1.1. Sensitivity of Calculated 2π sr Fluxes to Input Parameters

[16] According to the protocol for the model calculations some of the input parameters required by the RT models were freely chosen by the model operators. Having available model results based on different combinations of these parameters, their relative importance in the model-derived downwelling 2π sr fluxes can be quantitatively estimated.

[17] The ET solar spectrum may affect the calculated fluxes either in absolute sense or by introducing wavelength

structure in the spectra. The structure is caused by the convolution of the actual wavelength variability of the solar spectrum with the spectral resolution of the instrument used to measure it. Consequently, spectra derived from different instruments will have different spectral characteristics. Since atmospheric transmission is generally a smooth function of wavelength, the spectral characteristics of the ET spectrum are transferred more or less directly to the calculated spectra at the ground. An example is presented in Figure 1a, which shows the spectral difference of 2π sr fluxes as derived by the BM2 and UMU models. BM2 uses the ATLAS-3 solar spectrum up to 407.8 nm, then the ATLAS-2 up to 419.9 nm, and from then on the solar spectrum taken from Modtran 3.5. On the other hand, UMU uses ATLAS-3 up to 400 nm and above that the ET spectrum by *Neckel and Labs* [1984]. In the region where the two models use the same solar spectrum ($\lambda < 400$ nm) their difference is a smooth function of wavelength, whereas for $\lambda > 400$ nm it becomes noisy. In this particular example the differences induced by the ET spectra vary with wavelength from a few percent up to ~15%. The marked, but rather smooth, wavelength dependence of their difference in the ultraviolet B (UV-B) is mainly caused by the different ozone cross sections used by the two models (see Table 2). This suggestion is supported by their difference both for direct and global irradiance, which show similar behavior in magnitude, shape, and structure.

[18] A possible error related to the ET solar spectra used by the models might arise from differences in the wavelength scale considered by the model with respect to the wavelength scale of the ET spectrum. The scale in some of the published ET solar spectra (e.g., ATLAS-3) refers to wavelengths in a vacuum, while in most models the radiative transfer calculations are done with respect to air wavelengths. To convert an ET spectrum from vacuum to air, its wavelength scale must be shifted toward shorter wavelengths by a wavelength-dependent amount, which on average is ~0.1 nm (at normal temperature and pressure) for the UV region. Such a shift may produce remarkable structure in the spectral differences between two otherwise identical models, especially near the steep absorption lines of the solar spectrum. As an example, the difference between two spectra derived by the ACD and KNM models is shown in Figure 1b. Both models used the ATLAS-3 solar spectrum up to 400 nm and the one by *Neckel and Labs* [1984] at longer wavelengths, but ACD did not apply the correction for air wavelengths. Thus their difference up to 400 nm appears very noisy with deviations of up to 10% at individual wavelengths, while from 400 to 700 nm it is remarkably smooth. The significant curvature of the difference at around 600 nm is caused by KNM not accounting for the absorption by ozone in the Chappuis band, while the increasing deviation with decreasing wavelength in the UV-B is a result of the different ozone absorption cross sections used by the two models. The solid line on Figure 1b is the difference between 2π sr fluxes calculated by the Tropospheric Ultraviolet and Visible (TUV) V4.0 model using the original ATLAS-3 solar spectrum and the one corrected for air wavelengths. This difference varies about zero with deviations following very closely the structure of the difference between ACD and KNM up to 400 nm.

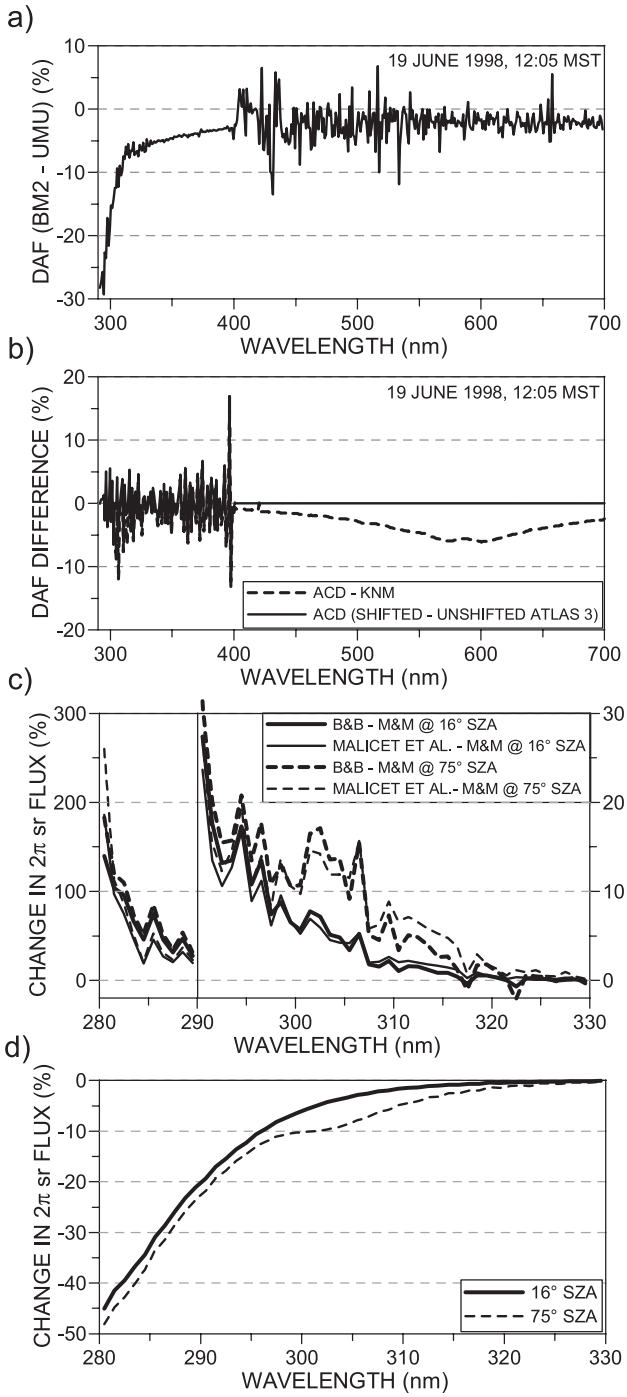

Figure 1. (a) Spectral difference in 2π sr fluxes (DAF) calculated by the BM2 and UMU models using different combinations of extraterrestrial solar spectra. (b) Spectral differences (dashed line) of 2π sr fluxes calculated by the ACD and KNM models using the ATLAS-3 spectrum up to 400 nm. In ACD, ATLAS-3 was not corrected to air wavelengths. The solid line represents the difference between two runs of the TUV model with the shift-corrected and the original, uncorrected ATLAS-3 solar spectrum. (c) Change in spectral 2π sr fluxes at 16° and 75° solar zenith angle (SZA) due to different ozone absorption cross sections. Note the scale change at 290 nm. (d) Change in spectral 2π sr fluxes at 16° (solid line) and 75° (dashed line) SZA caused by 2% increase in ozone column.

[19] Below 340 nm, where the ozone absorption is strong, the source for the ozone cross sections used in RT modeling becomes very important. From the IPMMI model results the effect of the different ozone cross sections can be identified in the calculated fluxes, but it is difficult to be isolated and quantified, because other parameters are also affecting the fluxes in this spectral region. Thus a separate set of calculations, outside the campaign protocol, was carried out using the LibRadtran code (B. Mayer, personal communication, 2002). Spectral 2π sr fluxes were calculated for two solar zenith angles and for two different values of total ozone using three different ozone absorption cross sections. Spectral differences of the fluxes based on *Bass and Paur* [1985] and *Malicet et al.* [1995] cross sections from those based on *Molina and Molina* [1986] were calculated and presented in Figure 1c.

[20] The *Bass and Paur* [1985] based fluxes are higher compared with those based on *Molina and Molina* [1986] throughout the UV-B region. The difference increases almost exponentially with decreasing wavelength, exceeding 30% below 290 nm. Between 300 and 310 nm, an important region for the $j(O^1D)$ calculations, the differences average to ~4% for small solar zenith angles, increasing to ~11% at 75° SZA. The fluxes based on cross sections by *Malicet et al.* [1995] are similar to those based on *Bass and Paur* [1985].

[21] Figure 1d shows the expected change in 2π sr fluxes for a 2% increase in total ozone, from 300 to 306 DU. This is the difference between the actual total ozone during the campaign and its value used in the modeling part of IPMMI, on the basis of the preliminary ozone data available at the time of the campaign [*Cantrell et al.*, 2003]. The effect of this small change in the ozone column becomes more important at large solar zenith angles, reaching −10% at 300 nm. Interestingly, below ~295 nm the effect of SZA becomes weaker, being only 3% different from changes calculated for 16° SZA. A similar effect in the same spectral region can be observed in Figure 1c, as an effect of different ozone cross sections. The absorption of radiation by ozone is proportional to the product of the ozone density and the absorption cross section, and hence the same change on either of the two parameters will produce the same effect on the transmitted radiation.

2.1.2. Description of the Radiative Transfer (RT) Models

[22] Several types of models, which are described in detail in the scientific literature, were used in this study. To assist the assessment of their results here, a brief description is given below. Models that were used by more than one group are presented only once.

[23] Three groups, ACD, KFU, and NOA, used three different versions, 4.0, 3.9, and 3.8, respectively, of the TUV model developed by S. Madronich (http://www.acd.ucar.edu/TUV/, 2002) using the discrete ordinates radiative transfer (DISORT) solver [*Stamnes et al.*, 1988] modified for pseudospherical geometry using Lagrangian interpolation between layers [*Petropavlovskikh*, 1995] and different combinations of input parameters as described in Table 2. All used atmospheric profiles from the *National Oceanic and Administration* (*NOAA*) [1976] for midlatitude summer, which were combined with vertical profiles of ozone, temperature, and pressure as measured on 19 June 1998.

[24] The AES model is based on pseudospherical geometry with a matrix operator doubling and adding code, which is used to produce lookup tables of j values for the Canadian general circulation model (middle atmosphere model). Details of the model structure can be found in the work of *de Grandpré et al.* [2000].

[25] The LibRadtran model (available at http://www.libradtran.org) used by NIL and BMx is a versatile radiative transfer package for calculation of radiation in the Earth's atmosphere. It includes various radiative transfer equation solvers as used by BMx [e.g., *Mayer et al.*, 1998], and also various ozone cross sections may readily be used; for example, BMx used *Molina and Molina* [1986], while NIL used *Bass and Paur* [1985]. *Mayer et al.* [1997] and *Kylling et al.* [1998] have extensively compared the package against measurements.

[26] The British Antarctic Survey Radiative Transfer Model (BASRTM), used by BAS, is built around the DISORT code of *Stamnes et al.* [1988] and the pseudospherical approximation of *Dahlback and Stamnes* [1991]. These calculations were performed using 16 streams and 50 computational layers of varying thickness. The atmospheric and ozone vertical profiles were those of the *NOAA* [1976], adjusted for local surface pressure and applying stratospheric scaling to the ozone column. Other input parameters were as defined in the protocol for model calculations. *Gardiner and Martin* [1997] present a more-detailed description and applications of the model.

[27] The JHU/Applied Physics Laboratory radiative transfer model used by the JHU group is based on algorithms originally developed by *Meier et al.* [1982] and *Anderson* [1983]. In this model, direct solar deposition and reflection from the surface are calculated in a spherical, refracting atmosphere, while multiple scattering is provided by an integral equation solution for the radiation field via a matrix inversion technique, assuming isotropic scattering in a plane parallel atmosphere (the pseudospherical approximation). Aerosol optical properties have been taken from the Modtran database [*Berk et al.*, 1989] and scaled to match the variable, measured 1020-nm AOD during IPMMI. The aerosol properties used had a smaller Angstrom coefficient than that suggested by the IPMMI aerosol measurements and a correspondingly lower AOD at shorter wavelengths. Variants of the JHU model have been primarily used for j value calculations in the stratosphere [e.g., *Swartz et al.*, 1999; *Swartz*, 2002]. Its principal product is the 4π sr actinic flux, but the model has been adapted here to approximate the 2π sr downwelling radiation field effecting photolysis at the Earth's surface.

[28] The Anisotropic Radiative Transfer (ART) code used by the KFA group is based on a multidirectional treatment of the diffuse radiation at 130 wavelengths ranging from 186 to 730 nm at variable intervals between 1 and 10 nm. The atmosphere is divided into 1-km layers from 0 to 100 km and the model considers absorption by O_2, O_3, and NO_2 and attenuation by Rayleigh and Mie scattering with four aerosol modes. It uses an analytical integration of the Beer-Lambert law under the condition of a constant source function within one layer. At each level an iterative approach with three iterations is used to solve the equation system [*Roeth*, 2002].

[29] The radiative transfer model, Doubling-Adding Koninglijk Nederlands Meteorologish Instituut (KNMI) (DAK), which was used by KNM, is an application of the doubling-adding method [*van de Hulst*, 1980] to polarized radiative transfer in the Earth's atmosphere. The extension that is currently in use at KNMI is described by *De Haan et al.* [1987]. The model consists of a shell of atmospheric optical properties around a doubling-adding radiative transfer kernel. The atmosphere consists of an arbitrary number of plane parallel layers, each of which has molecular scattering, gas absorption, and aerosol scattering and absorption. Monochromatic calculations without polarization are made to obtain the spectral actinic flux at the surface over the spectral range 280–700 nm with 1-nm steps. Polarization is assumed to be of minor importance for calculation of the surface fluxes. Aerosol profiles are assumed constant in boundary layer, troposphere, and stratosphere, respectively. All fluxes are normalized values, assuming an incident solar irradiance of unity at the top of the atmosphere. Calculations of the diurnal cycle are made very fast because the doubling-adding code allows for simultaneous evaluation of the radiative transfer for a set of solar zenith angles.

[30] The radiative code used by LOA is based on pseudospherical successive orders of scattering (SOS). The equation of transfer is solved iteratively for the radiation scattered one, two, or n times. The source function is computed for the photons scattered n times from the photons scattered $(n - 1)$ times, starting with the analytical source function for single scattering; 15 iterations are sufficient for all wavelengths in a cloudless atmosphere. The inhomogeneous atmosphere is approximated by the superposition of 22 homogeneous layers, of 1 km in the lower levels and 5 km in the higher levels. The angular integrations necessary to compute the source function, as well as the final actinic flux and irradiance, are performed with a 20-point Gaussian quadrature. Details of the code can be found in Appendix A of *Sherlock et al.* [1999].

[31] MAR uses a parameterization scheme for photolysis rate calculation in three-dimensional atmospheric models. First, the actinic flux profiles are approximated at seven wavelengths (205, 288, 302, 309, 320, 370, and 580 nm), using a very simple parameterization and some reference profiles calculated with the DISORT code (eight streams used). Actinic fluxes are calculated as a function of the solar zenith angle, the cloud optical thickness above/below (Mie scattering), the air column above/below (Rayleigh scattering), the ozone column above/below (ozone absorption), and the surface albedo. This scheme does not account for aerosol effects or for atmospheric curvature. From the actinic fluxes, photolysis frequencies are constructed using effective cross sections, which are derived either from simple functions of the local temperature or from look up tables. This part of the calculation is described in *Landgraf and Crutzen* [1998].

[32] In the OPT model the atmosphere is assumed to be plane stratified with pseudospherical correction and with scattering according to Rayleigh's law [*Bates*, 1984], IPMMI reference ozone profile, and prescribed surface albedo. The solution method is based on the successive iteration of the auxiliary equation of the radiative transfer [*Dave*, 1964, 1965; *Dave and Furukawa*, 1966]. The calculations of atmospheric transmission are done at the original sampling wavelengths of the ozone cross sections measured by *Bass and Paur* [1985] (shifted to vacuum, steps ~0.05 nm). The transmittance values were linearly interpolated to the vacuum wavelengths of the high-resolution ET solar flux data (ATLAS-2 and ATLAS-3 Solar Ultraviolet Spectral Irradiance Monitor (SUSIM) ET spectra combined with Modtran 3.5 solar flux for wavelengths longer than 419.9 nm) and multiplied by the ET spectrum (after Sun-Earth distance correction). Next, the wavelengths were shifted to air (standard temperature-pressure conditions). Finally, high-resolution surface flux values (in absolute units) were slit-averaged with a 1-nm rectangular filter function and reported at the IPMMI standard grid.

[33] The model that was used by UMU is System for Transfer of Atmospheric Radiation (STAR) [*Ruggaber et al.*, 1994] in its present version (H. Schwander et al., System for Transfer of Atmospheric Radiation (STAR), version 1999, available at http://www.meteo.physik.uni-muenchen.de/strahlung/uvrad/Star/starprog.html, 1999). The model is developed at the Meteorological Institute of the University of Munich using Matrix Operator Theory [*Nakajima and Tanaka*, 1988]. The effects of atmospheric curvature are approximated with the pseudospherical method. Aerosol is taken into account on the basis of mixtures of components [*Hess et al.*, 1998], with its properties depending on relative humidity and wavelength. The aerosol type that was used for the calculations was "clean continental," with much lower absorption and smaller increase of AOD toward shorter wavelengths than suggested. Ozone absorption cross sections are taken from Global Ozone Monitoring Experiment (GOME) reference measurements [*Burrows et al.*, 1999].

2.1.3. Justification of Revisions of RT Model Results

[34] For Johns Hopkins University (JHU) a more accurate interpolation and integration of the O_3 and NO_2 cross sections and quantum yields (particularly in wavelength regions where molecular parameters or the solar flux vary exponentially) was adopted to make better use of the relatively high wavelength resolution employed during IPMMI. A correction was applied for an error in the code that derives the horizontal surface irradiance from flux calculations, which was added for the intercomparison. Finally, the generic aerosol profile used in the initial submission was modified by the total aerosol extinction that was measured at the surface during the campaign, in order to account more accurately for the diurnal variability of the aerosol loading.

[35] Because of confusion about the definition of "spectral direct irradiance" (normal to the beam), the originally submitted NOA data for this category were weighted by the cosine of the solar zenith angle, i.e., the irradiance incident on a horizontal plane. The NOA data were resubmitted with the cosine dependence removed.

[36] The original model calculations by the OPT group were done for an aerosol-free atmosphere using LOWTRAN7 ET solar flux spectrum. The model results were later revised to include aerosol corrections for each actinic flux component (direct, diffuse, and reflected) and prescribed IPMMI aerosol parameters using the radiative transfer model of *Herman et al.* [1995]. The ET solar flux data were also changed to a more recent data set (ATLAS-3

SUSIM measurements; see Table 2). Since the ET solar flux and ozone cross sections in the OPT model were referred to wavelengths in vacuum, the submitted results were finally shifted to air wavelengths.

[37] Initial comparisons between the OPT results and the mean of the other models revealed errors in modifications made to the interface of the RT code, which resulted in erroneous ozone absorption coefficients. Consequently, the fluxes that were calculated for wavelengths shorter than ~320 nm were significantly underestimated. This illustrates the usefulness of such intercomparison activities. Before submitting results corrected for these errors, three additional details of the computations were addressed: an improved ET solar flux (changes <5%), the inclusion of aerosol attenuation/scattering (changes <10%), and the shifting of model calculations to an air wavelength scale from a vacuum scale (significantly reducing the standard deviation of the model-measurement spectral differences).

[38] The UMU results were submitted for a second time, without any change in the model and the atmospheric description, since at certain ranges of wavelengths of the initially submitted data set the radiation quantities were zeros. It was impossible to find the reasons for which this information vanished when the calculations were submitted to the referee.

2.2. Spectral Measurements

[39] Four spectroradiometers provided spectral solar radiation measurements during the IPMMI experimental campaign; three of them (Forschungszentrum Juelich (FZJ), National Center for Atmospheric Research (NCAR) and University of Leicester (ULI)) measured the spectrum of the downwelling solar actinic flux (2π sr), and the fourth (National Institute of Water and Atmospheric Research (NIWA)) measured the global irradiance on a horizontal surface. The entrance optics of the first three instruments were installed ~5 m above the ground on towers mounted on top of the sea containers to ensure 180° free field of view. The NIWA spectroradiometer was positioned on the ground with its diffuser ~2 m above surface and at a distance from the other instruments sufficient to ensure an unobscured view. The actinic flux spectroradiometers are equally sensitive to radiation from any angle of incidence (even from directions close to the horizon) and therefore their field of view is very important. In the irradiance spectroradiometer the incoming radiation is weighted by the cosine of the angle of incidence and therefore the contribution of radiation from large zenith angles is relatively small.

[40] The group of the Institute of Atmospheric Chemistry in Juelich, Germany, operated the FZJ spectroradiometer. The instrument consists of a 2π sr actinic flux head (quartz diffuser of 37 mm height), a scanning double monochromator (Bentham DTM 300), a photoelectric detection system (EMI 9250 photomultiplier operating in current measurement mode), and a PC for data acquisition and system control. A new head, which was constructed in a similar way to the one described in *Hofzumahaus et al.* [1999], was used in the IPMMI campaign, accompanied by a shadow ring of 300 mm in diameter serving as an artificial horizon. The angular sensitivity to incident radiation was measured in the laboratory with a point radiation source and was found to be almost constant (±3%) for polar angles between 0° and 85°. Between 85° and 90°, sensitivity drops by 8% and reaches zero between 90° and 105°. The diffuser was mounted on a mast on the roof of the container and was connected to the spectrometer, operating inside the container in a temperature-stabilized environment (35 ± 1°C), with a 10 m quartz fiber bundle.

[41] Spectra of 2π sr fluxes were scanned from 280 to 420 nm at steps of 1 nm and a spectral band pass (FWHM) of 1.1 nm. The scanning time was typically 68 s, whereas the total acquisition time for each spectrum was 80 s. The time base for this instrument was a GPS receiver, which maintained the time to within 1 s.

[42] The wavelength calibration of the instrument was controlled by scanning the emission lines of a low-pressure mercury lamp and by comparison of the wavelength structure of the measured spectra with the Fraunhofer structure of the solar spectrum. Throughout the campaign the calibration was stable to within 0.05 nm and accurate to within ±0.1 nm. Before and after the campaign (on 17 and 20 June, respectively) the spectroradiometer was calibrated for absolute 2π sr flux measurements in the laboratory sea container against a standard of spectral irradiance (FEL 1000-W quartz halogen lamp made by Gigahertz Optik GmbH, traceable to PTB standards) following the procedure outlined by *Hofzumahaus et al.* [1999]. Post campaign checks performed in Juelich, Germany, showed that this lamp agreed to better than 1.0% with two different standards of spectral irradiance. During the campaign, working standard lamps of 200 W were used to check the stability of the spectroradiometer's sensitivity on 18 and 19 June. From all lamp measurements it was determined that the sensitivity of the instrument between 17 and 20 June was within 2%.

[43] The NCAR Scanning Actinic Flux Spectroradiometer is described in full by *Shetter and Mueller* [1999]. As installed during IPMMI, the spectroradiometer measures downwelling actinic flux as a function of wavelength. The computer-automated instrument is based on a small, lightweight, double monochromator with photomultiplier tube and a signal amplifier, connected by a fiber optic bundle to a 2π sr light collector. Scans from 280 to 420 nm were made every 15 s (starting on the minute) by stepping in 1.0-nm increments from 280 to 330 nm and 2.0-nm increments from 330 to 420 nm. The time was routinely set to a GPS receiver to remain synchronous with the other IPMMI instruments. The mean time for those wavelengths associated with $j(O(^1D))$ was ~3 s after the scan start and 6 s for $j(NO_2)$. Calibrations were performed every few days to ensure wavelength stability and to track changes in the spectral sensitivity of the instrument, details of which are given by *Cantrell et al.* [2003].

[44] For the measurement of 2π sr actinic-flux spectra, the University of Leicester group used a new single monochromator diode-array spectroradiometer system. The instrument collects photons isotropically (within ~2%) across the 2π sr solid angle using a polished quartz dome/diffuser arrangement. Detected photons were then passed through a round-to-slit converter (70 μm × 2500 μm) giving a spectral band pass of ~2 nm FWHM. Photons entering the entrance slit are dispersed using a flat field diffraction grating (2400 lines/mm) and detected using a 512-pixel diode array (Carl Zeiss). The manufacturer-quoted wavelength drift for this arrangement was 5×10^{-4} nm/K. The

wavelength scale was calibrated using a low-pressure Hg discharge lamp (Oriel). Spectra were collected over the wavelength region 280–450 nm at four integration times (0.5, 1, 3, and 5 s) and converted to actinic flux using National Institute of Standards and Technology (NIST)-traceable (irradiance) calibration standards. ULI used for its absolute calibration the same standard of spectral irradiance as NCAR, and thus its absolute calibration is not absolutely independent. A full instrument characterization is given by *Edwards and Monks*, [2003].

[45] As seen in the description above, the scanning time for recording one spectrum was different for each of the three instruments, but for all was <2 min. To achieve comparability with respect to the timing of their measurements, each spectroradiometer provided spectra averaged over 10 min, which were formed from all spectra recorded during this interval. The time assigned to each spectrum was the middle of the 10-min interval.

[46] The NIWA instrument [*McKenzie et al.*, 1992] is based on a commercially available J-Y DH10 double monochromator of 100-mm focal length, configured for additive dispersion to measure the spectral irradiance falling on a horizontal surface. Since its development in 1990, the instrument has been used continuously and has participated successfully in international intercomparisons [e.g., *Seckmeyer et al.*, 1995]. Recent modifications include replacement of the original diffuser with an in-house-designed polytetrafluoroethylene diffuser coupled to the instrument via a fiber optic bundle and enclosing the instrument in a weatherproof temperature-stabilized enclosure. In the IPMMI campaign the spectrometer scanned the spectral range 290–450 nm with a sampling step of 0.2 nm and at a spectral resolution of ~1.3 nm at FWHM. The scan duration was ~3 min, with a repetition interval of 5 min. The detector is an EMI 9804QA photomultiplier operated in analog mode. Calibrations are with respect to NIST, with an estimated uncertainty of ±6%. During the campaign the NIWA spectrometer was set up with its diffuser 2 m above the ground.

[47] The irradiances provided include small correction factors, $cf(\lambda, \mathrm{SZA})$, to account for departures from a true cosine response in the diffuser. These corrections take the form

$$cf = cf_{\mathrm{sky}} D + cf_{\mathrm{sun}}(1 - D), \tag{3}$$

where D is the diffuse fraction, defined as the ratio of diffuse/global irradiance, cf_{sky} is the correction factor for the sky radiation (assumed to have an isotropic distribution), and cf_{sun} is the correction factor for direct sunlight. The diffuse fraction D was calculated using a simple single-layer radiative transfer model [*McKenzie et al.*, 2002]. The diffuser on the NIWA instrument has an excellent cosine response, with $cf_{\mathrm{sky}} = 1.012$ and $|(cf_{\mathrm{sun}} - 1)| < 0.03$ for all SZA < 70°. At larger SZA, cf_{sun} increases and exceeds 1.2 by SZA = 85°.

3. Comparison of Radiative Transfer Model Results

[48] Because of the large dynamic range in the solar radiation received in the ultraviolet, resulting mainly from absorption by stratospheric ozone, an efficient way to compare several spectra produced by RT models or measured by spectroradiometers is to investigate their level of agreement against a single spectrum, which may serve as a reference for the comparison. In order to be able to expose any subtle differences between the sample spectra, the reference spectrum chosen must at least share the fundamental characteristics of these spectra. Ideally, the reference spectrum would describe the actual solar spectrum at the instant of the measurement or calculation, but obviously this cannot be known. Even a well-calibrated and well-maintained spectroradiometer provides only a representation of the true solar spectrum, on the basis of its response to solar radiation relative to an artificial radiation source.

[49] For the case of the modeling part of IPMMI (involving comparisons of a large number of spectra) an average spectrum derived from all model results could serve as an adequate reference. To avoid introducing a bias into this average by including unrepresentative outlying spectra, the reference for this study was formed using only a subset of the available data. Such a reference may still be biased if the majority of model results included in it were based on an erroneous input parameter. However, provided that the reference is used only to expose the relative differences between the model results and is not regarded as possessing any absolute validity, any such bias will be unimportant. Measured spectra could also be used as a reference for the model intercomparison, but then the accuracy of the input parameters used in the models would become significant. For instance, on the basis of the preliminary data supplied the models were run using an ozone column ~2% higher than the actual, thus introducing an error. When comparing the modeled spectra with a reference spectrum taken from the measured results, this error may mask more subtle deviations between the models at shorter UV wavelengths.

[50] Outlying spectra were excluded using the following iterative process: From each spectrum the integral of the flux between 300 and 400 nm was calculated and compared to the average flux derived from all models. At each cycle of the iteration those spectra for which the integrated flux was different by more than 0.5σ of all fluxes forming the average were removed. This criterion was chosen more or less arbitrarily, ensuring only that the reference was formed by spectra from at least one third of the models and that none of them deviated significantly from the others. The models used to form the reference were identified only from the spectra close to local noon, and the same models were used for all eight case studies (hourly from 0505 to 1205 LT), assuming that if a model misbehaves at small solar zenith angles, it would be probably be worse at larger ones. Similar methodologies, involving more sophisticated algorithms, were used in the past in intercomparison campaigns of ultraviolet spectroradiometers [e.g., *Gardiner and Kirsch*, 1997; *Bais et al.*, 2001]. The following nine models were selected through this process: ACD, AES, BM1, BM2, BM3, KFA, KNM, LOA, and NIL. Their results were simply very close to each other, and they should not necessarily be regarded as representative of the actual solar spectrum at the specific instant. After examining the reference for the different observation times it appeared that at large solar zenith angles the KFA results were extremely different from the other eight, and hence KFA was removed

from the list. Having established the comparison reference for each of the eight observation times, the percentage deviations of all spectra from the corresponding reference were computed. It should be noted again that the comparability among model results could be assessed from these deviations only in a relative sense.

[51] Figure 2 shows comparisons of all model-derived spectra of 2π sr flux at two solar zenith angles, 16° (close to local noon) and 75°, as percentage deviations from the respective comparison norms. Because of the large number of the spectra, only a qualitative picture of the agreement among the models can be perceived from Figure 2. At noon it appears that all models agree quite well (to within ~10% in the visible), while the agreement worsens with decreasing wavelength, becoming about ±15% in the UV-B. At wavelengths below 300 nm the modeled spectra become so noisy that no firm conclusions can be safely derived. This noise is a combined effect of differences in the wavelength structure of ET solar spectra, absorption cross sections, and the algorithms used by the different models to solve the radiative transfer equation. The encouraging perception of the agreement that emerges from Figure 2 (left) is true only for small solar zenith angles, since at larger ones (Figure 2, right) the models start deviating progressively and at 0505 LT (85° SZA) some models depart by more than 100%, especially at the shorter wavelengths. Such behavior could be a consequence of the assumption that the atmosphere is plane parallel and thus not properly accounting for the important effects of the Earth's curvature on the transfer of solar radiation through the atmosphere. A second reason for the large discrepancies at large solar zenith angles could be the different ozone absorption cross sections used by the various models. With increasing solar zenith angle, scattering and absorbing processes gain in significance (longer radiation path), so a difference in the inputs, e.g., in the aerosol amount or the vertical ozone distribution, will result in higher differences between the models. The most striking differences are found in the results of KFA, MAR, and NOA, which deviate from the others by more than 10% in the entire spectral region, while KNM departs mainly in the visible, because it does not take into account the ozone absorption in the Chappuis band. This effect is evident mostly at large solar zenith angles due to the increased ozone absorption in the enhanced path length of radiation.

[52] From Figure 2 one can also see distinct spikes and dips, which are caused mainly by differences in the wavelength structure of the ET solar spectra used by the models (see Table 2 and Figures 1a and 1b). This structure is transferred more or less directly to the calculated spectra at the ground, since the atmospheric transmission is generally a much smoother function of wavelength.

[53] Obviously, Figure 2 provides only a general picture about the agreement among different models. For a more detailed assessment of their performance the investigation will be restricted to individual wavelengths and more specifically on averages over narrow wavelength bands, which significantly reduce the spectral noise. Two spectral bands were chosen, each one 5 nm wide and centered at 310 nm and at 400 nm, which were considered representative of the 2π sr fluxes used in the calculation of photolysis frequencies for O_3 to $O(^1D)$ and NO_2 to $O(^3P)$, respectively. The percentage departures of the 2π sr fluxes produced by the

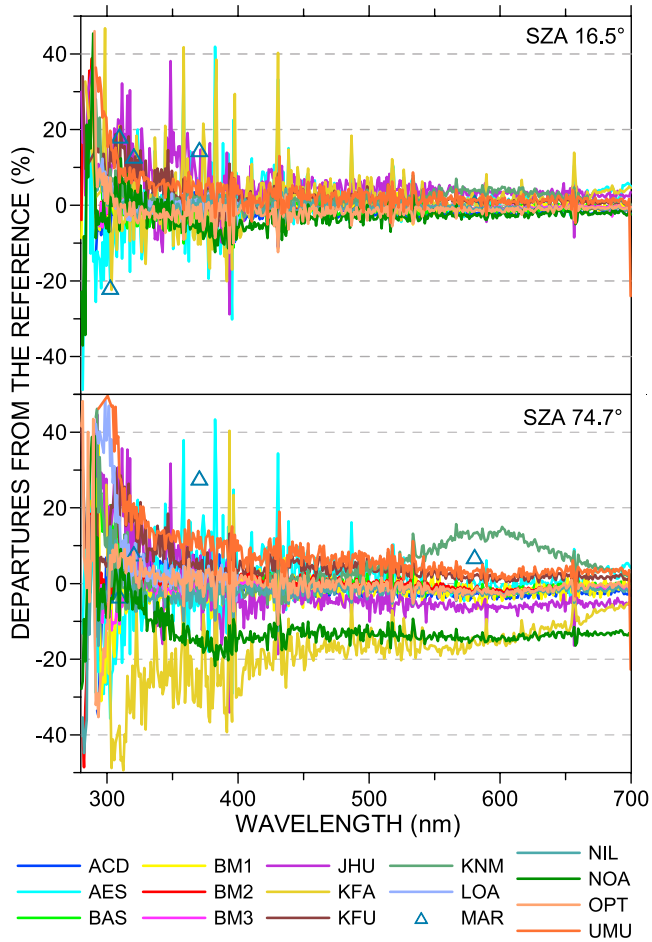

Figure 2. Percentage departures of model-derived spectra of downwelling (2π sr) actinic flux from the comparison reference at (top) high and (bottom) low solar elevations for Marshall field, Boulder, Colorado, on 19 June 1998.

16 models from the reference (Model-Reference)100/Reference are presented in Figure 3 as a function of SZA. The solar zenith angle during this time period ranged from 85° at 0505 LT to 16° at 1205 LT. In general, the models agree better in the ultraviolet A (UV-A) than in the UV-B region (e.g., to within ±2.8% and ±5.7%, respectively, at 40.6° SZA). For both wavelength bands almost all models deviate progressively with increasing solar zenith angle, and in a few cases (MAR, UMU, and KFA) the deviations for the first observation (85° SZA) at 310 nm are even higher than 50%, so the corresponding data are excluded from Figure 3. Recall that the models that formed the comparison norm were chosen according to their relative agreement at noontime and with respect to the 2π sr flux integral between 300 and 400 nm. The contribution of the lower UV-B wavelengths (e.g., for $\lambda < 310$ nm) to this integral is practically negligible. If regarded in an absolute sense, even the models entering the reference may deviate significantly from the reference spectrum at large solar zenith angles and at short UV-B wavelengths. Therefore only the relative agreement between models can be safely assessed from the results of Figure 3.

[54] At 310 nm, 11 models (those forming the reference and BAS, NOA, and OPT) agree very well, to within ~5–6% for solar zenith angles smaller than 63°. At the two

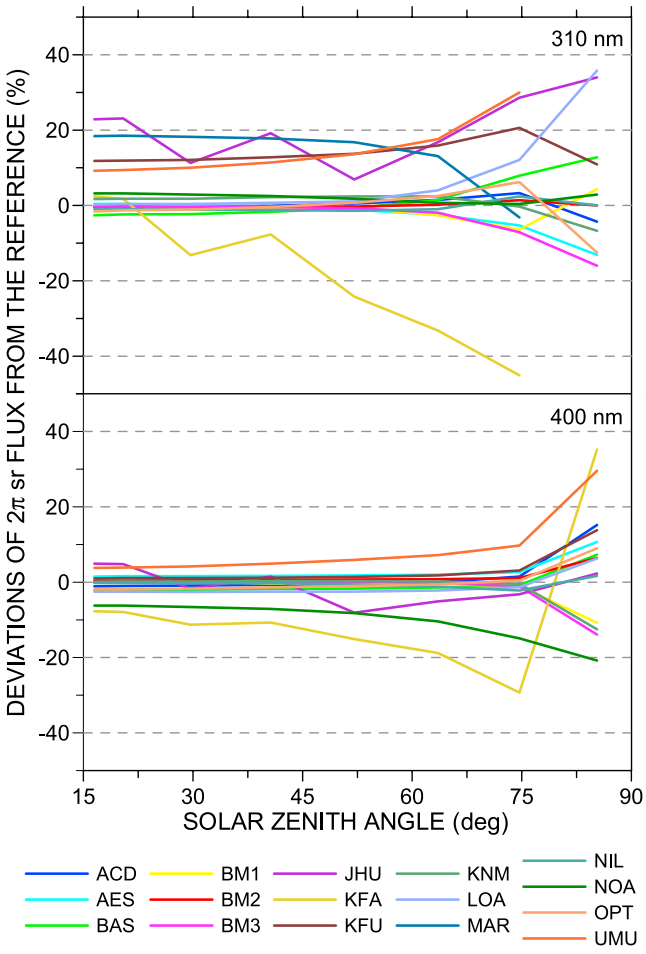

Figure 3. Departures of downwelling (2π sr) solar actinic fluxes, calculated by different models for 19 June 1998, from the comparison reference at two selected, 5-nm-wide, wavelength bands centered at (top) 310 nm and at (bottom) 400 nm as a function of SZA.

earliest observation times, which correspond to ~85° and 75° SZA, only five models (ACD, BM2, KNM, NIL, and NOA) are still clustered to within ~6%, while the others deviate up to 15% about the zero line. With the exception of KNM the results forming this group were produced by only two codes (TUV and LibRadtran), which were run by different groups, using different model atmospheres. The reason for the large deviations at large solar zenith angles is not obvious, and it is probably the combined effect of various parameters, including the ozone absorption cross sections, the treatment of the curvature of the atmosphere, the vertical structure of the atmospheric layers, etc. The vertical profiles of ozone and aerosols that could produce such effects are unlikely to contribute, because the ozone profile was given from measurements, and the aerosol vertical structure is unimportant when the total optical depth is low. The use of ozone cross sections by *Bass and Paur* [1985] instead of those by *Molina and Molina* [1986] results in an overestimation of the 2π sr flux at SZA of 85° by 3–5% at 310 nm, increasing to ~10% at 300 nm. UMU was the only model using GOME O_3 cross sections [*Burrows et al.*, 1999], resulting in even stronger deviations but in the same direction, because these cross sections are similar to those by *Bass and Paur* [1985] but with finer resolution. Moreover, the high values calculated by UMU both at 310 and 400 nm, and their increase with decreasing wavelength and increasing SZA, result from the low aerosol absorption that was used (SSA = 0.96 instead of 0.5) and the lower-Angstrom coefficient (a = 1.1 instead of 1.7), which results in lower AOD at shorter wavelengths. The disagreement of KFU cannot be explained by the O_3 cross sections or by the ET solar spectrum, because other models use the same input parameters without deviating so much from the reference.

[55] The results of the JHU model at 310 nm and at small SZA are significantly larger than the reference, in part as a result of using the Modtran 3 ET spectrum, which was ~6% higher than ATLAS at this wavelength. Although a constant value of the AOD (0.03 at 550 nm) for the entire day was provided for the modelers, the JHU group used the AOD measurements at 1020 nm made during the campaign using a handheld Microtops II Sun photometer. Most of the marked structure in the model differences as a function of SZA can be attributed to the use of the variable aerosol optical depth, ranging from 0.02 to 0.18 at 550 nm. In addition, the use of aerosol parameters other than those specified to the modelers (SSA = 0.94 instead of 0.5, g = 0.65 instead of 0.45, and a between 0.8 and 0.9 instead of 1.7) is also responsible for part of the absolute difference in the JHU model. These differences were evaluated with separate runs of the JHU model, including one that followed the exact, constant aerosol specification of the IPMMI campaign [*Swartz*, 2002]. Finally, the large departures of KFA and MAR results are probably a combined effect of the input parameters and the RT codes, which, according to Table 2, are different from all other models.

[56] The situation is much better for all models at 400 nm, as now all but four models (JHU, KFA, NOA, and UMU) agree to within ~7% for SZA smaller than 75°. The deviations of the JHU model are on the average also within ~7%, but they again exhibit a SZA-dependent structure for the reasons discussed above. Results from the MAR model do not appear in Figure 3 since this model provides estimates only at specific wavelengths, the highest wavelength being 370 nm. Similar to the previous case, at 85° SZA the models diverge significantly, forming two or three distinct groups. Since no ozone absorption occurs in this wavelength region, the most likely reason for the large deviations would be again a combination of ET solar spectra and RT codes but also the treatment of the wavelength variation of surface albedo. With regard to the three other quantities (global and direct irradiance and 4π sr actinic flux), the model results have behavior similar to the one shown in Figure 3, with small differences in the absolute deviations, emerging from the differences in the geometry of the radiative transfer.

[57] Since the selected wavelengths for the discussion coincide with the regions where the photolysis frequencies for O_3 to $O(^1D)$ and NO_2 to $O(^3P)$ are sensitive, similar results must be expected with respect to $j(O(^1D))$ and $j(NO_2)$ model estimates from the radiation point of view. Differences in the photolysis frequencies may also arise from the different temperatures, cross sections, and quantum yields used for the calculation [e.g., *Shetter et al.*, 1996].

[58] From the comparisons presented so far it can be concluded that the agreement among different models depends strongly on wavelength and solar zenith angle, and almost all models tend to agree within a few percent in the UV-A and visible and at small solar zenith angles. At individual wavelengths, significant differences may occur mainly because of the use of different ET solar spectra. However, these differences are suppressed when averages over spectral bands a few nanometers wide are compared. The models have difficulty producing consistent results at large solar zenith angles, partly due to the use of different ozone absorption cross sections and partly due to differences in handling the radiative transfer of diffuse radiation under the assumption of a plane parallel atmosphere. Nevertheless, only a few models are exceptionally different, while the rest agree to better than ±10%. A benchmark of 12 models that was carried out within the EC Scientific UV Data Management project [*van Weele et al.*, 2000] showed differences between the models of ~10% at 310 nm due to different handling of the curvature of the atmosphere. Besides these differences the agreement between the models was in the order of 3% or less for wavelengths higher than 310 nm, because in that model comparison, all input parameters required by the models were strictly defined. Many of the models that took part in that benchmark were also present in the IPMMI exercise.

4. Comparison of Measured Spectral Actinic Solar Fluxes

[59] Three of the spectroradiometers that took part in the IPMMI campaign made spectral measurements of downwelling actinic flux in the ultraviolet, which were recorded as 10-min averaged spectra every hour from 0505 to 1205 LT. Examples of the spectra reported for 1205 LT (the observation closest to local noon) are shown in Figure 4. A logarithmic scale was used owing to the large dynamic range of the measurements at the shorter UV-B wavelengths. The first point to note is that the measurements of the FZJ and NCAR instruments follow each other closely, while the measurement of ULI deviates significantly, at least over three broad spectral regions. The overestimate of its measurements at the short wavelengths by 2–3 orders of magnitude is a clear signature of stray light contamination. The smaller deviations in the other spectral regions (~350 and ~420 nm) are probably due to instrument sensitivity or stability problems [see also *Edwards and Monks*, 2003]. For wavelengths longer than 400 nm a software setup problem caused the significant disagreement with the other two instruments.

[60] A closer look at the spectra of the other two instruments reveals differences mainly in the fine wavelength structure, which cannot easily be discerned in Figure 4. By computing the percent difference between spectra recorded at the same time by the two instruments, the effect of the dynamic range is suppressed, and the actual differences become detectable. Differences between NCAR and FZJ spectra are shown in Figure 5 (top) for all available observational times, confirming the sense of agreement that was suggested by Figure 4. There are two important features in Figure 5: first, the repeatable wavelength structure of the differences, which weakens the overall agreement between the two instruments to within about ±15% and, second, a

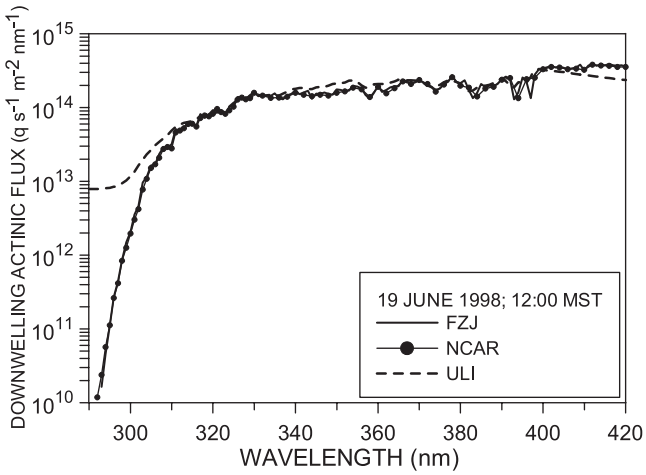

Figure 4. Spectra of downwelling (2π sr) actinic flux as measured by the FZJ, NCAR, and ULI spectroradiometers on 19 June 1998 at Marshall field, Boulder, Colorado. Time is given in Mountain Standard Time (MST).

kind of diurnal change in the absolute level of the differences, which is clearer at the longer wavelengths. With the exception of the first spectrum of the day, obtained at 85° SZA, the difference decreases regularly when moving from morning hours toward noon, indicating changes in the sensitivity of one or both instruments. The most common reasons for such a diurnal variation of the sensitivity are temperature effects, nonlinear response of the detector, and effects of the angular sensitivity of the entrance optics. Imperfect leveling of the entrance optics cannot play the significant role it does in irradiance measurements.

[61] A full day comparison of photolysis frequencies derived from the spectra of these two instruments (A. Hofzumahaus et al., Photolysis of O_3 to $O(^1D)$: Measurements and modeling during the International Photolysis Frequency Measurement and Modeling Intercomparison (IPMMI) 1998, submitted to *Journal of Geophysical Research*, 2003) reveals that the diurnal difference of their measurements continues in the afternoon hours and is not symmetric about local noon. Therefore one may exclude from the possible reasons the nonlinearity of the detector. Because the NCAR instrument was temperature-controlled and the diurnal difference is not correlated with temperature, it is unlikely that the diurnal difference is a result of ambient temperature changes. This suggests that a nonideal angular response of the entrance optic may be the cause of this small diurnal difference. The particular entrance optic employed by the NCAR spectroradiometer during IPMMI does indeed have a very good angular response at the two azimuth angles tested prior to IPMMI. However, further testing in the new automated NCAR angular calibration facility revealed a nonsymmetric angular response error on the order of 3–4% at certain azimuth angles, which may explain some of this diurnal trend in the FZJ/NCAR ratio. More discussion on the sensitivity of NCAR spectroradiometer is provided by *Shetter et al.* [2003].

[62] Spectral differences of the ULI from the FZJ instrument are shown in Figure 5 (middle). Because of the known stray light problem of ULI, the differences at the short UV-B wavelengths are very large, and the corresponding

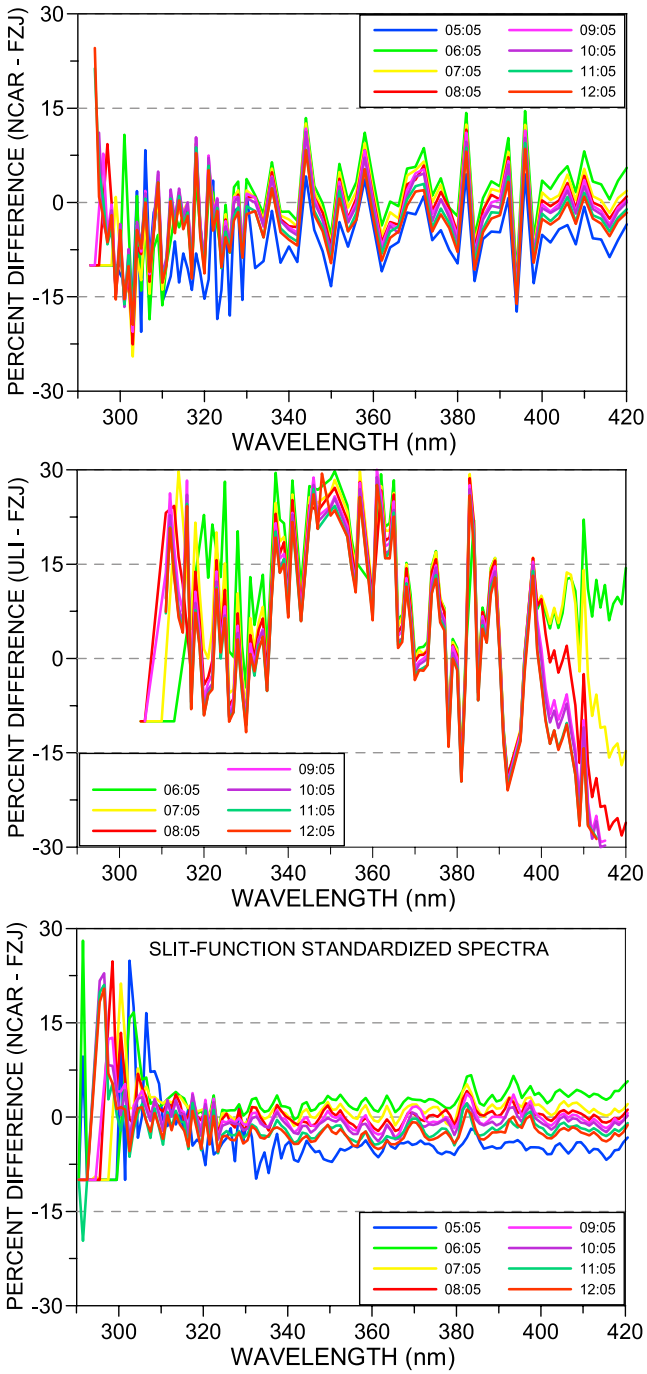

Figure 5. Percent spectral differences of downwelling (2π sr) actinic flux measured at Marshall field, Boulder, Colorado, on 19 June 1998, by (top) NCAR and (middle) ULI spectroradiometers from simultaneous measurements by FZJ. (bottom) Difference between NCAR and FZJ after their spectra were standardized to a triangular slit function of 1 nm at spectral band pass.

data points were not plotted. The truncation wavelength varies with solar zenith angle, ranging between 318 nm at 0605 LT and 308 nm at 1205 LT. Regardless of the strong wavelength-dependent disagreement of the two instruments, their difference in the spectral region between 350 and 400 nm is remarkably stable during the day.

[63] The spectral structure in the difference between NCAR and FZJ is mainly due to the different spectral resolutions of the two instruments, both in the shape of their slit function and the band pass. The response of a spectroradiometer at a given wavelength is actually the integral of the solar spectrum at the ground weighted by the shape of its slit function. Therefore the response of each instrument at the same wavelength is expected to be different, especially in regions with significant natural wavelength structure of the ambient radiation, as, e.g., near the Fraunhofer lines or at the steep part of the spectrum (UV-B) caused by the ozone absorption. The actual slit function of each spectroradiometer (although usually approximated with a triangle) has a unique and rather complex shape, which results in a unique representation of the measured spectrum with respect to wavelength structure. Thus spectra recorded by two different instruments are never identical. Through the application of deconvolution and convolution techniques a measured spectrum can be modified to resemble the response of an instrument with a different slit function, usually of simpler shape, like a triangle. Such a methodology has been developed by H. Slaper [*Slaper et al.*, 1995] and has been extensively used in various intercomparison campaigns of ultraviolet spectroradiometers in the last 5 years [e.g., *Bais et al.*, 2001]. This algorithm (SHICrivm) was applied to all spectra measured by the NCAR and FZJ instruments to derive spectra standardized to a common 1-nm-wide spectral resolution. Although a triangular slit function is usually considered as ideal, in this study a rectangular slit function was used to achieve comparability between the measurements and the model calculations. The application of SHICrivm requires an ET solar spectrum at fine resolution and sampling step and the slit function of the spectroradiometer at fine steps as well. In this study the solar spectrum measured at Kitt Peak was used [*Kurucz et al.*, 1984], and the slit functions of the spectroradiometers were provided by their operators, determined by scanning a mercury line at fine steps.

[64] The differences between the standardized spectra of NCAR and FZJ are given in Figure 5 (bottom). The structure seen in Figure 5 (top) has disappeared, and the small remnants are probably due to combined uncertainties in the measurement of the slit functions in the laboratory, in the finite resolution of the Kitt Peak spectrum and in the SHICrivm algorithm itself. The most dramatic change has occurred in the UV-B region, which shows an improvement, as now the differences are almost wavelength-independent, at least above 305 nm. The disagreement in the region <305 nm is probably caused by the reduced accuracy of the measurements due to low signal and also by the reduced accuracy in the SHICrivm performance at these short wavelengths. The diurnal variation in the UV-A, evident from Figure 5 (top), is still present since the standardization process of the spectra does not affect their absolute magnitude. Overall, this procedure improved the agreement between NCAR and FZJ to better than ±6% at all solar zenith angles and ±3% for SZA < 60° and wavelengths >310 nm.

[65] The SHICrivm algorithm is also able to detect wavelength shifts in the measured spectra, by comparison of their wavelength structure to the structure of the solar spectrum outside the atmosphere, and to apply the necessary corrections. In the FZJ spectra the shifts that were deter-

mined were <0.03 nm, so their effect can be considered as negligible. This suggests that the Fraunhofer line wavelength corrections applied by FZJ were quite successful. The analysis of the wavelength shifts for the unmodified NCAR spectra revealed wavelength shifts as large as 0.3 nm. While this shift may be considered large for spectral measurements, its effect in integrals is rather small. For example, a 1-nm wavelength shift in the UV-B region of the spectra will produce an error of at most 21% in the calculated $j(O^1D)$. However, a 1-nm wavelength error in the UV-A will result in only a 1.7% error in $j(NO_2)$ [*Cantrell et al.*, 2003]. The NCAR spectra were not corrected for wavelength shifts, and this is probably the reason for the observed wavelength shifts. From the above discussion it seems necessary to recommend the use of techniques like SHICrivm of Fraunhofer structure comparisons on measured actinic flux spectra for improving their accuracy.

[66] In conclusion, it appears that the measurements of FZJ and NCAR agree to within ±6% for all solar zenith angles with no wavelength dependence for $\lambda > 300$ nm. At shorter wavelengths either NCAR overestimates or FZJ underestimates the 2π sr flux by up to 20% at 300 nm. From the available information and measurements it is not possible to say which of the two assumptions is correct. As concerns the ULI measurements, its large deviations (up to ±30%) with respect to the other two instruments for $\lambda > 310$ nm suggest a major problem in the absolute calibration of the instrument, despite its rather stable response throughout the day in the 350- to 400-nm spectral region. Below 310 nm the deviations are much larger due to poor stray light rejection.

[67] A fourth spectroradiometer (NIWA) was in operation during the experimental campaign, providing spectra of solar irradiance on a horizontal surface. Its spectra are not comparable with the downwelling 2π sr actinic flux spectra of the previous three spectroradiometers, simply because they represent a different radiometric quantity. However, under certain assumptions, mainly of isotropic distribution of the diffuse radiation, the irradiance measurements of NIWA were converted to 2π actinic fluxes. The methodology that was followed has been recently tested in similar studies using modeling and experimental results [e.g., *Kazadzis et al.*, 2000; *Hofzumahaus et al.*, 1999] and is described in more detail by *McKenzie et al.* [2002].

[68] Under clear skies with a SZA of 60°, the irradiance measured by the NIWA instrument was approximately half of the actinic flux, as predicted by simple theory, giving confidence in the radiometric calibration accuracy of the other three spectral instruments. Comparisons between the NIWA instrument and the other spectral instruments also showed that under the observation conditions that prevailed during the campaign, ozone photolysis frequencies $j(O_3)$ could be estimated from the irradiances with uncertainties of 10–20% for SZA less than ~85°. However, the errors in estimating NO_2 photolysis frequencies $j(NO_2)$ under cloudy conditions were significantly larger, on the order of 30% [*McKenzie et al.*, 2002].

5. Comparison of Modeled and Measured Spectral Actinic Solar Fluxes

[69] The spectra produced by the models are in principle directly comparable since they were calculated for the same wavelength range and step size and for the same spectral resolution (1 nm). On the other hand, comparisons between measured spectral fluxes are much more difficult since the individual optical characteristics of the spectroradiometers (e.g., slit function and wavelength step) have a direct influence on the shape and structure of the reported spectra. Therefore the standardized measured spectra were used in the comparison with the modeled spectra, as has been already described in section 4. Through this standardization the measured spectra are modified to match the wavelength step and spectral resolution of the models. The uncertainty introduced by this procedure is expected to be rather small, depending mainly on how accurately the slit function of the spectroradiometer is determined [*Slaper et al.*, 1995].

5.1. Downwelling Actinic Fluxes

[70] From the discussion of section 4 it became evident that the FZJ and NCAR spectroradiometers behaved similarly, and either of them could serve as a reference for comparing the spectral measurements. From those two instruments the FZJ was chosen for the comparisons to follow, mainly for three reasons: first, due to its narrower slit function, which leads to smaller errors in the standardization process; second, because the slit function provided by its operators was better described (larger dynamic and wavelength ranges) than that of NCAR; and, third, because of its better wavelength stability, as reported from the SHICrivm analysis. The FZJ spectra were standardized to 1-nm resolution, to match the resolution of the models, and hence their spectral difference from the modeled spectra is expected to have insignificant wavelength structure. Spectral percentage departures of 2π sr fluxes derived by each model from the corresponding measured spectrum by FZJ were produced for three selected solar zenith angles (~75° (0605 LT), 52° (0805 LT), and 16° (1205 LT)) and are shown in Figure 6 in separate plots for each model.

[71] From the plots of Figure 6 it appears that in most cases the differences depend on solar zenith angle and this dependence becomes stronger with decreasing wavelength. In the UV-A, where no ozone absorption occurs, half of the models (BM1, BM2, BM3, KFA, JHU, KNM, NOA, and NIL) underestimate the 2π sr fluxes at 75° SZA (0605 LT). On the other hand, ACD, AES, BAS, KFU, UMU, and, to a lesser extent, LOA and OPT are remarkably consistent with the measurements at all three SZA to within only a few percent, suggesting that it would be unlikely that the measurements are responsible for the SZA dependence. The reason for the differences seen in the first group of models is not clear. It is most likely a combined effect of different factors; for example, the assumption of a plane parallel atmosphere in the treatment of diffuse radiation, which dominates the 2π sr flux at large solar zenith angles, as well as the choices made by the modelers for the unknown input parameters required by their models.

[72] In the UV-B the agreement is worse and in most cases SZA-dependent with deviations ranging between 5 and 20%. In a few models (BAS, LOA, and UMU) the deviations from the measurements are smaller and considerably less dependent on solar zenith angle. Such a behavior points to the absorption of UV radiation by ozone, which depends on the ozone column and the absorption cross sections used in the model. The total ozone that was provided for input to

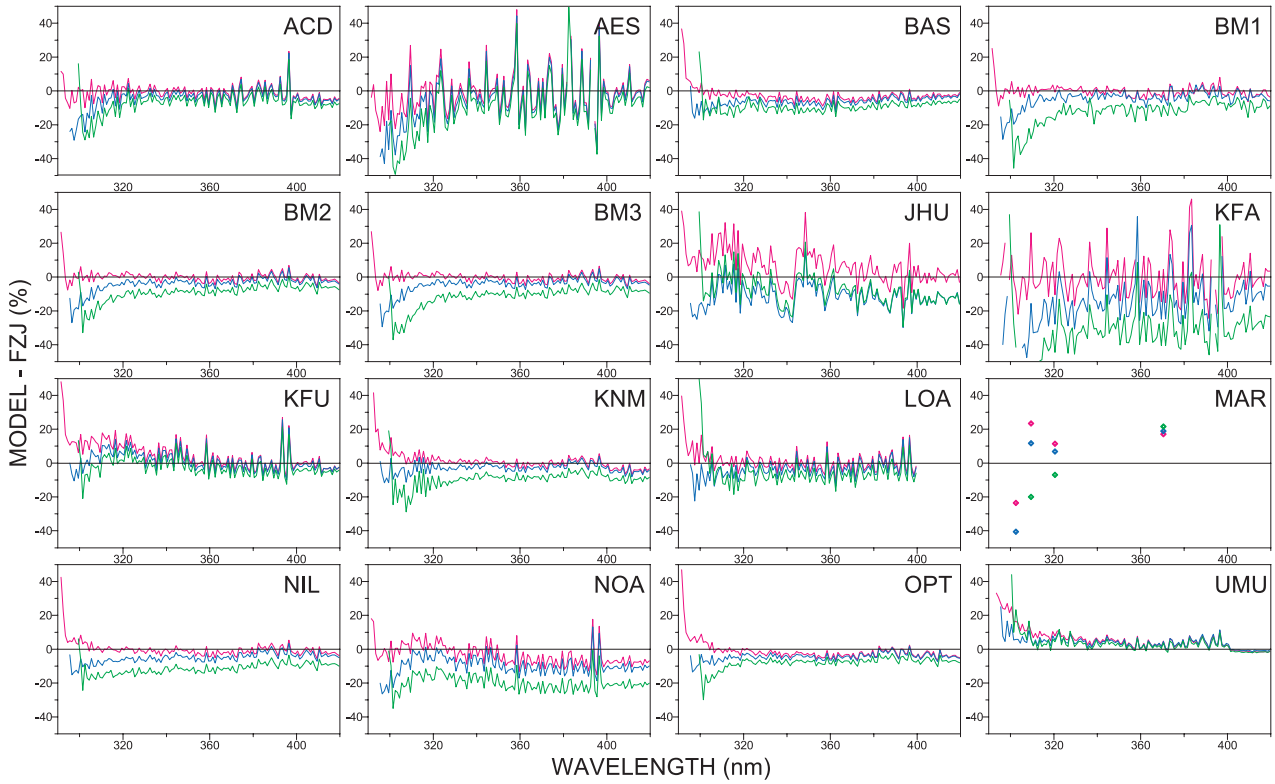

Figure 6. Spectral differences of model-derived downwelling (2π sr) fluxes from the measurements of FZJ spectroradiometer performed at 0605 LT, 75° SZA (green line), 0805 LT, 52° SZA (blue line), and 1205 LT, 16° SZA (red line) at Marshall field, Boulder, Colorado, on 19 June 1998.

the models was indeed overestimated by ~2%, which resulted in underestimating the 2π sr flux at 75° SZA by ~10% at 300 nm and by 5% at 310 nm (see Figure 1d). In addition, the uncertainty in the ozone column measurements, although it is generally small, may explain a small part of the differences between model results and measurements. However, for some models (ACD, BM1, BM2, BM3, and NOA) the deviations are still larger than those explained by the ozone column difference. All these models use the same O_3 absorption cross sections, by *Molina and Molina* [1986]. After the recommendation of the World Meteorological Association (WMO) in 1992 the calculation of total ozone is based on the *Bass and Paur* [1985] scale, and therefore it would be reasonable to expect that model calculations based on different cross sections would show differences, especially in the region of strong ozone absorption. On the other hand, the deviations of the models that use the *Bass and Paur* [1985] O_3 cross sections in the UV-B should be more consistent with their behavior in the UV-A. This is confirmed in Figure 6 by the results of LOA, NIL, KNM, KFU, OPT, BAS, and UMU, the latter two using O_3 cross sections by *Malicet et al.* [1995] and GOME [*Burrows et al.*, 1999], respectively, which are quite similar to those by *Bass and Paur* [1985]. Figure 1c suggests that ~10% increase in 2π sr flux at 300 nm and at 75° SZA should be expected when the *Bass and Paur* [1985] cross sections are used instead of those by *Molina and Molina* [1986]. Thus one may conclude that for most models the observed differences from the measurements in the UV-B region can be explained by the two contentions discussed above.

[73] At local noon and for wavelengths above 315 nm, five models (BM1, BM2, BM3, KNM, and NIL) agree with the measurements on the average to within 1% ± 2.5%. The average deviation for ACD and LOA is within 1%, but the marked wavelength structure increases the standard deviation of the departures to 4.7% and 5% respectively. What is common in these seven models is the use of ATLAS-3 solar spectrum in their calculations. Thus their good agreement with the measurements could be regarded as a confirmation of the appropriateness of that solar spectrum in the model calculations, taking into account that in this spectral region, effects from the ozone absorption are insignificant. In fact, of the other models, ATLAS-3 was used only by OPT, which only marginally failed to be included in the previous group because its average deviation from the measurements was −2.3%, and by UMU, which overestimates the 2π sr flux by ~3.5%. Most clearly for UMU, but also for ACD and KNM, a step at 400 nm can be seen. At 400 nm all three models change the solar spectrum from ATLAS-3 to *Neckel and Labs* [1984]. A comparison of both solar spectra with the Kitt Peak solar spectrum from 360 nm to 440 nm, carried out by H. Schwander (personal communication, 2002), shows that the differences against *Neckel and Labs* [1984] for wavelengths above 400 nm are negligible, whereas ATLAS-3 is ~3% high for wavelengths below 400 nm.

[74] At wavelengths below 300 nm the noise in the measurements is expected to increase, and, consequently, the comparisons become worse. A closer look at the first few wavelengths (e.g., for $\lambda < 295$ nm) reveals that for

almost every model, there are positive deviations from the measurements (even at local noon). This suggests that at these first wavelengths the spectroradiometric measurements are underestimated, perhaps due to the low signal that is close to the detection limit of the instruments and errors induced by the subtraction of the dark signal, which is comparable to the real signal.

[75] In almost all model results, there are notable negative deviations from the measurements, which increase with increasing SZA and decreasing wavelength. In addition to the reasons discussed in the previous paragraphs, this behavior can be imposed also by mistreatment of the multiple scattering when a model assumes a plane parallel atmosphere. Such an indication is given by the different behavior of BM2 and BM3 models, which differ only in their RT algorithm. BM3 uses the original DISORT parameterization, while BM2 uses its pseudospherical version. Because of this difference, at 75° SZA, BM2 has larger deviations with respect to BM3, ranging from 1 to 2% in the UV-A up to 10% close to 300 nm. However, this discussion applies only to two models, BM2 and KNM, providing insufficient information for fully analyzing the effect of this assumption on the calculated fluxes.

[76] The AES, JHU, and KFA models present remarkable but repeatable wavelength structure, occasionally differing from the measurements by up to ±40%. There are indications that the structure in AES and KFA is probably caused by wavelength interpolations used in the codes, since such large departures cannot be explained by the ET solar spectra. In particular, the scatter of the KFA differences is believed to be due to the uneven wavelength calculation in the ART model. Most probably, the interpolation formula was not adequate to describe accurately the wavelength structure of the spectrum. A separate comparison with the FZJ spectroradiometer data, without applying any interpolation to the data, showed much less scatter. The wavelength structure in the JHU results, and the large departures from the measurements, are largely the effect of using the Modtran 3 ET spectrum, which none of the other models have used. Particularly between 340 and 350 nm the departures from the measurements are due almost entirely to the use of the Modtran 3 spectrum. The use of variable AOD by the JHU group (see section 3) is probably the cause for the large differences seen between the noon and the morning spectral differences.

[77] Finally, the comparisons with the MAR model were restricted to the four available wavelengths. This showed a rather poor agreement, both in terms of wavelength and solar zenith angle dependence, with deviations ranging from about −30% to +20%.

[78] Similar conclusions are derived from the comparisons of the models with the NCAR measurements (not shown here). Only at the shorter UV-B wavelengths ($\lambda <$ 300 nm) does the agreement become worse, as expected from the results presented in Figure 5 (bottom). This indicates that the NCAR spectroradiometer is responsible for the small disagreement between FZJ and NCAR in this wavelength region. The combined analysis of the measurement intercomparison and the comparisons of model calculations with measurements helped in uncovering (at least partly) the reasons for the observed differences.

5.2. Irradiance Measurements

[79] Similar to Figure 6, Figure 7 shows differences of irradiance on a horizontal surface (global irradiance) as calculated by the models from that measured by the NIWA spectroradiometer. Although the general picture is the same between the Figures 6 and 7, there are differences that are worth mentioning. In the irradiance results the solar zenith angle dependence is considerably smaller for all models. The main differences between the two cases are, first, the contribution of the diffuse radiation from directions close to the horizon being almost negligible in the global irradiance with respect to 2π sr flux and, second, the contribution of the direct beam which in the global irradiance is scaled by the cosine of the SZA. However, at large solar zenith angles the direct component is strongly attenuated at the UV wavelengths, and hence most of the difference must be due to diffuse radiation. This might suggest that the models can handle more accurately the diffuse radiation from directions close to the zenith than close to the horizon. The agreement between the models and the measurements is generally slightly better in Figure 7 than in Figure 6, even at local noon. Models agree with the measurements of NIWA to within ∼9% at 300 nm and ∼2.5% at 400 nm for solar zenith angles up to ∼60°. With regard to the wavelength dependence the results of Figures 6 and 7 are almost identical, as the sources of the wavelength structure are the ET solar spectra used by the different models.

6. Conclusions

[80] The model and measurement intercomparisons and the model-to-measurement comparisons of spectral fluxes in the framework of IPMMI contributed significantly to uncovering the causes of differences among models and measurements. The set of model input parameters obtained from measurements reduced the uncertainty in the model calculations and enabled the investigation of the importance of the remaining input parameters required by the models. In some cases, model developers used the results of the comparisons to investigate in depth the weaknesses of their models and improve their capabilities.

[81] The observed differences among the models were attributable mainly to input data, such as the ET solar flux and the ozone absorption cross sections, but also to the assumption of plane parallel atmospheric structure, which leads to poor modeling of the scattered radiation. The agreement among model calculations becomes worse with increasing solar zenith angle, due to enhancement of the effects from the above-mentioned parameters. Significant wavelength structure can be observed in the differences between models as a result of the different resolution of the ET spectra. For SZA smaller than 75°, most of the models (ACD, AES, BM1, BM2, BM3, KFA, KNM, LOA, NIL, BAS, and OPT) agreed with each other to within ±7% in the UV-A and visible and within about ±10% in the UV-B, and only one or two models had significant differences from the measured 2π sr actinic fluxes.

[82] The intercomparison of measurements from the three spectroradiometers FZJ, NCAR, and ULI proved that the first two agree to within ±6%, independent of solar zenith angle and wavelength region. The significant role of spectral resolution in the comparability of the instruments

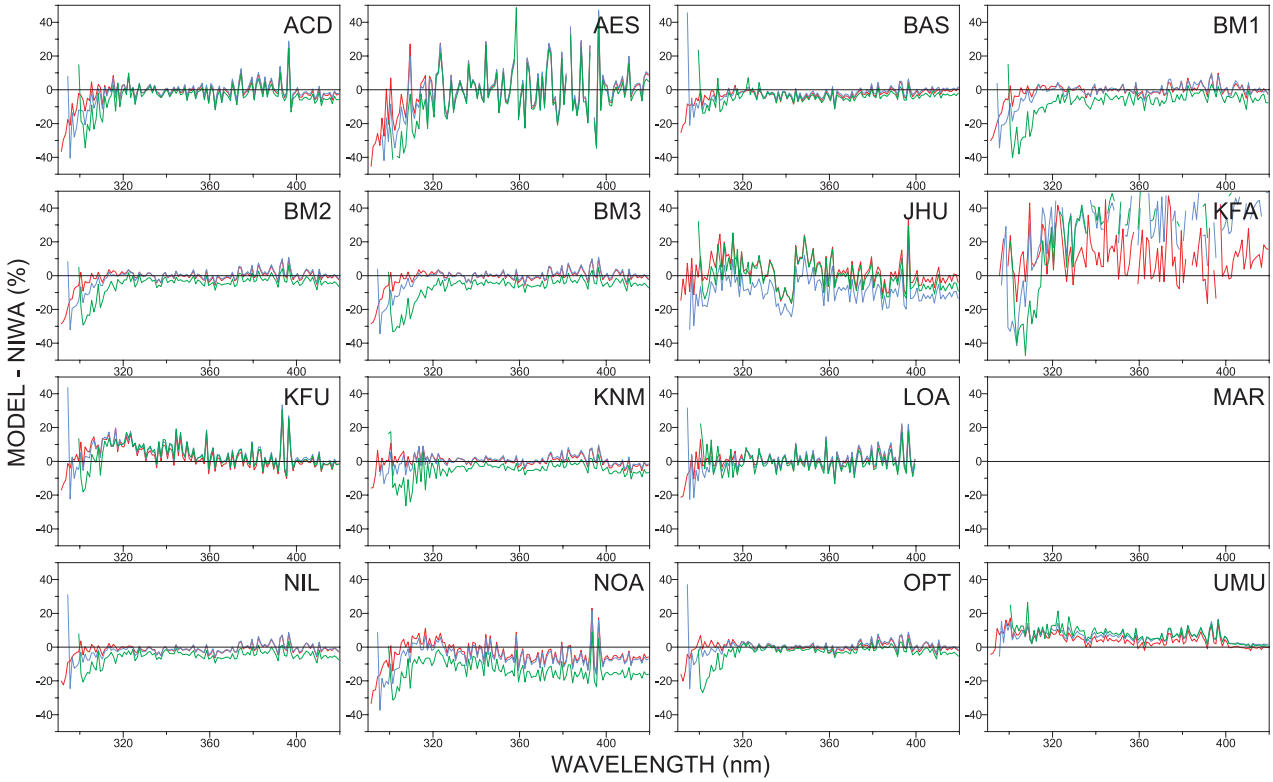

Figure 7. Spectral differences of model-derived irradiances on a horizontal surface from the measurements of NIWA spectroradiometer performed at 0605 LT, 75° SZA (green line), 0805 LT, 52° SZA (blue line), and 1205 LT, 16° SZA (red line) at Marshall field, Boulder, Colorado, on 19 June 1998.

was demonstrated through the remarkable improvement in their agreement (from ±15 to ±6%) when their spectral measurements were standardized (deconvolved and reconvolved) to a common spectral resolution. The ULI instrument, being a single monochromator, suffered from stray light and absolute calibration problems, which caused significant disagreements (up to ±30%) with the two double-monochromator spectroradiometers, practically at all wavelengths. However, when integrated values (such as photolysis frequencies) are used, the performance of the instrument is better [*Edwards and Monks*, 2003].

[83] The comparisons of model calculations with the spectral measurements (both 2π sr flux and irradiance) showed that most models were in reasonable agreement with the measurements. It is of interest that models, although deviating significantly from the reference in the model-to-model comparison, agree satisfactorily with the measured spectra in the model-to-measurement comparison. This could be a consequence of the way the reference was formed, dominated by a set of models with similar behavior, which despite their agreement do not necessarily represent the true solar spectrum at the ground. The agreement of a few percent in the UV-A and at local noon becomes worse with decreasing wavelength toward the UV-B and increasing solar zenith angle. The fact that models that used the ATLAS-3 ET solar spectrum are in better agreement with the measurements suggests the appropriateness of ATLAS-3 for model calculations. This hypothesis is further supported by independent model runs which showed that when all model input parameters except the ET solar spectrum are the same, the calculated actinic flux spectrum based on ATLAS 3 compares better with the measurements at the ground in the region 300–400 nm than those based on Modtran 3 and *Neckel and Labs* [1984]. *Ritter et al.* [1987] suggested that most of the tested ET solar spectra could be used for $j(O^1D)$ calculations safely since the observed deviations are comparable with the measurements' uncertainties. However, ATLAS-3 was not included in that study.

[84] The improvement in the agreement between models and measurements in the case of global irradiance suggests that the models, and possibly the measurements, have difficulty handling accurately the diffuse radiation from directions close to the horizon. The findings from the comparisons point to the need for quantification of the uncertainties introduced into the model results from input parameters such as the ET solar spectra and the absorption cross sections of ozone, which are among the main sources of uncertainties in modeling of UV radiation.

[85] **Acknowledgments.** This study was partly supported by WMO/UMAP as an activity of the Modeling Subgroup of the WMO Scientific Advisory Group (SAG) on UV Monitoring and by the National Science Foundation and the National Center for Atmospheric Research.

References

Anderson, D. E., Jr., The troposphere-stratosphere radiation field at twilight: A spherical model, *Planet. Space Sci.*, *31*, 1517–1523, 1983.

Arvesen, G. P., R. N. Griffin Jr., and B. D. Pearson Jr., Determination of extraterrestrial solar spectral irradiance from a research aircraft, *Appl. Opt.*, *8*, 2215–2232, 1969.

Bais, A. F., et al., SUSPEN intercomparison of ultraviolet spectroradiometers, *J. Geophys. Res.*, *106*, 12,509–12,526, 2001.

Bass, A. M., and R. J. Paur, The ultraviolet cross-sections of ozone: I, II, in *Atmospheric Ozone, Proceedings of the Quadrennial Ozone Symposium Held in Halkidiki, Greece, 3–7 September 1984*, edited by C. S. Zerefos and A. Ghazi, pp. 606–616, D. Reidel, Norwell, Mass., 1985.

Bates, D. R., Rayleigh scattering by air, *Planet. Space Sci.*, *32*, 785–790, 1984.

Berk, A., L. S. Bernstein, and D. C. Robertson, Modtran: A moderate resolution model for LOWTRA0N 7, *Tech. Rep. GL-TR-89-0122*, Geophys. Lab., Air Force Syst. Command, Hanscom Air Force Base, Hanscom, Mass., 1989.

Burrows, J. P., A. Richter, A. Dehn, B. Peters, S. Himmelmann, S. Voigt, and J. Orphal, Atmospheric remote sensing reference data from GOME-2, Temperature dependent absorption cross-sections of O_3 in the 231–794 nm spectral range, *J. Quant. Spectrosc. Radiat. Transfer*, *61*, 509–517, 1999.

Cantrell, C. A., J. G. Calvert, A. F. Bais, R. E. Shetter, B. L. Lefer, and G. D. Edwards, Overview and conclusions of the International Photochemical Measurement and Modeling Intercomparison (IPMMI) Study, *J. Geophys. Res.*, *108*(D16), 8542, doi:10.1029/2002JD002962, in press, 2003.

Crawford, J., R. Shetter, B. Lefer, C. Cantrell, W. Junkermann, S. Madronich, and J. Calvert, Cloud impacts on UV spectral actinic flux observed during IPMMI, *J. Geophys. Res.*, *108*(D16), 8545, doi:10.1029/2002JD002731, in press, 2003.

Dahlback, A., and K. Stamnes, A new spherical model for computing the radiation field available for photolysis and heating at twilight, *Planet. Space Sci.*, *39*, 671–683, 1991.

Dave, J. V., Meaning of successive iteration of the auxiliary equation in the theory of radiative transfer, *Astrophys. J.*, *108*, 338–346, 1964.

Dave, J. V., Multiple scattering in a non-homogeneous, Rayleigh atmosphere, *J. Atmos. Sci.*, *22*, 273–279, 1965.

Dave, J. V., and P. M. Furukawa, Scattered radiation in the ozone absorption bands at selected levels of a terrestrial, Rayleigh atmosphere, *Meteorol. Monogr.*, *7*(29), 353, 1966.

de Grandpré, J., S. R. Beagley, V. I. Fomichev, E. Griffioen, J. C. McConnell, A. S. Medvedev, and T. G. Shepherd, Ozone climatology using interactive chemistry: Results from the Canadian Middle Atmosphere Model, *J. Geophys. Res.*, *105*, 26,475–26,491, 2000.

De Haan, J. F., P. B. Bosma, and J. W. Hovenier, The adding method for multiple scattering calculations of polarized light, *Astron. Astrophys.*, *183*, 371–391, 1987.

DeLuisi, J. J., and C. L. Mateer, On the application of the optimum statistical inversion technique to the evaluation of Umkehr observations, *J. Appl. Meteorol.*, *10*, 328–334, 1971.

Edwards, G. D., and P. S. Monks, Performance of a single monochromator diode array spectroradiometer for the determination of actinic flux and atmospheric photolysis frequencies, *J. Geophys. Res.*, *108*(D16), 8546, doi:10.1029/2002JD002844, in press, 2003.

Elterman, L., UV, visible and IR attenuation for altitudes to 50 km, *AFCRL-68-0153*, *285*, Air Force Cambridge Res. Lab., Bedford, Mass., 1968.

Gardiner, B. G., and P. J. Kirsch, Intercomparison of ultraviolet spectroradiometers, in *Advances in Solar Ultraviolet Spectroradiometry*, edited by A. R. Webb, *Air Pollut. Res. Rep. 63*, pp. 67–151, Off. for Off. Publ. of the Eur. Communities, Luxembourg, 1997.

Gardiner, B. G., and T. J. Martin, On measuring and modelling ultraviolet spectral irradiance, in *IRS '96: Current Problems in Atmospheric Radiation: Proceedings of the International Radiation Symposium, Fairbanks, Alaska, 19–24 August 1996*, edited by W. L. Smith and K. Stamnes, pp. 917–920, A. Deepak, Hampton, Va., 1997.

Herman, B. M., T. R. Caudill, D. E. Flittner, K. J. Thome, and A. Ben-David, A comparison of the Gauss-Seidel spherical polarized radiative transfer code with other radiative transfer codes, *Appl. Opt.*, *34*, 4563–4572, 1995.

Hess, M., P. Koepke, and I. Schult, Optical Properties of Aerosols and Clouds: The software package OPAC, *Bull. Am. Meteorol. Soc.*, *79*, 831–844, 1998.

Hofzumahaus, A., A. Kraus, and M. Mueller, Solar actinic flux spectroradiometry: A technique for measuring photolysis frequencies in the atmosphere, *Appl. Opt.*, *38*, 4443–4460, 1999.

Kazadzis, S., A. F. Bais, D. Balis, C. S. Zerefos, and M. Blumthaler, Retrieval of downwelling UV actinic flux density spectra from spectral measurements of global and direct solar UV irradiance, *J. Geophys. Res.*, *105*, 4857–4864, 2000.

Kraus, A., and A. Hofzumahaus, Field measurements of atmospheric photolysis frequencies for O_3, NO_2, HCHO, CH_3CHO, H_2O_2 and HONO by UV spectroradiometry, *J. Atm. Chem.*, *31*, 161–180, 1998.

Kurucz, R. L., I. Furenlid, J. Brault, and L. Testerman, Solar flux Atlas from 296 to 1300 nm, in *National Solar Observatory Atlas 1*, Harvard Univ. Press, Cambridge, Mass., 1984.

Kylling, A., A. F. Bais, M. Blumthaler, J. Schreder, C. S. Zerefos, and E. Kosmidis, Effect of aerosols on solar UV irradiances during the Photochemical Activity and Solar Ultraviolet Radiation campaign, *J. Geophys. Res.*, *103*, 26,051–26,060, 1998.

Landgraf, J., and P. J. Crutzen, An efficient method for online calculations of photolysis and heating rates, *J. Atmos. Sci.*, *55*, 863–878, 1998.

Malicet, J., D. Daumont, J. Charbonnier, and C. Parisse, Ozone UV spectroscopy II: Absorption cross-sections and temperature dependence, *J. Atmos. Chem.*, *15*, 263–273, 1995.

Mayer, B., G. Seckmeyer, and A. Kylling, Systematic long-term comparison of spectral UV measurements and UVSPEC modeling results, *J. Geophys. Res.*, *102*, 8755–8767, 1997.

Mayer, B., A. Kylling, S. Madronich, and G. Seckmeyer, Enhanced absorption of UV radiation due to multiple scattering in clouds: Experimental evidence and theoretical explanation, *J. Geophys. Res.*, *103*, 31,241–31,254, 1998.

McKenzie, R. L., P. V. Johnston, M. Kotkamp, A. Bittar, and J. D. Hamlin, Solar ultraviolet spectroradiometry in New Zealand: Instrumentation and sample results from 1990, *Appl. Opt.*, *31*, 6501–6509, 1992.

McKenzie, R. L., P. V. Johnston, A. Hofzumahaus, A. Kraus, S. Madronich, C. Cantrell, J. Calvert, and R. Shetter, Relationship between photolysis frequencies derived from spectroscopic measurements of actinic fluxes and irradiances during the IPMMI campaign, *J. Geophys. Res.*, *107*(D5), 4042, doi:10.1029/2001JD000601, 2002.

Meier, R. R., D. E. Anderson Jr., and M. Nicolet, Radiation field in the troposphere and stratosphere from 240–1000 nm, I, General analysis, *Planet. Space Sci.*, *30*, 923–933, 1982.

Molina, L. T., and M. J. Molina, Absolute absorption cross sections of ozone in the 185- to 350-nm wavelength range, *J. Geophys. Res.*, *91*, 14,501–14,508, 1986.

Mueller, M., A. Kraus, and A. Hofzumahaus, O3 $\rightarrow$ O(^1D) photolysis frequencies determined from spectroradiometric measurements of solar actinic UV-radiation: Comparison with chemical actinometer measurements, *Geophys. Res. Lett.*, *22*, 679–682, 1995.

Nakajima, T., and M. Tanaka, Algorithms for radiative intensity calculations in moderately thick atmospheres using a truncation approximation, *J. Quant. Spectrosc. Radiat. Transfer*, *40*, 51–69, 1988.

National Oceanic and Amospheric Administration (NOAA), *U.S. Standard Atmosphere, 1976*, U.S. Govt. Print. Off., Washington, D. C., 1976.

Neckel, H., and D. Labs, The solar radiation between 3300 and 12500 Å, *Sol. Phys.*, *90*, 205–258, 1984.

Petropavlovskikh, I., Evaluation of photodissociation coefficient calculations for use in atmospheric chemical models, Ph.D. thesis, U. of Brussels, *NCAR Coop. Thesis 159*, Nat. Cent. for Atmos. Res., Boulder, Colo., 1995.

Ritter, J. A., D. H. Stedman, R. R. Dickerson, and T. E. Blackburn, Dependence of j[O3-O(^1D)] on the choice of extraterrestrial solar irradiance data, *Environ. Sci. Technol.*, *21*, 505–508, 1987.

Roeth, E.-P., Description of the anisotropic radiation transfer model ART to determine photodissociation coefficients, *Ber. Juel-3969*, Forschungszentrums Juelich, Juelich, Germany, 2002.

Ruggaber, A., R. Dlugi, and T. Nakajima, Modeling radiation quantities and photolysis frequencies in the troposphere, *J. Atmos. Chem.*, *18*, 171–210, 1994.

Schneider, W., G. K. Moortgat, S. Tyndall, and J. P. Burrows, Absorption cross sections of NO_2 in the UV and visible region (200–700 nm) at 298 K, *Photochem. Photobiol.*, *40*, 195–217, 1987.

Seckmeyer, G., et al., Geographical differences in the UV measured by intercompared spectroradiometers, *Geophys. Res. Lett.*, *22*, 1889–1892, 1995.

Sherlock, V., A. Hauchecorne, and J. Lenoble, Methodology for the independent calibration of Raman backscatter water-vapor lidar systems, *Appl. Opt.*, *38*, 5816–5836, 1999.

Shetter, R. E., and M. Mueller, Photolysis frequency measurements using actinic flux spectroradiometry during the PEM-Tropics mission: Instrument description and some results, *J. Geophys. Res.*, *104*, 5647–5661, 1999.

Shetter, R. E., C. A. Cantrell, K. O. Lantz, S. J. Flocke, J. J. Orlando, G. S. Tyndall, T. M. Gilpin, C. A. Fisher, S. Madronich, and J. G. Calvert, Actinometric and radiometric measurements of the photolysis rate coefficient of ozone to (O^1D) during Mauna Loa Observatory Photochemistry Experiment 2, *J. Geophys. Res.*, *101*, 14,631–14,461, 1996.

Shetter, R. E., et al., Photolysis frequency of NO_2: Measurement and modeling during the International Photolysis Frequency Measurement and Modeling Intercomparison (IPMMI), *J. Geophys. Res.*, *108*(D16), 8544, doi:10.1029/2002JD002932, in press, 2003.

Shettle, E. P., Models of aerosols, clouds and precipitation for atmospheric propagation studies, *AGARD Conf.*, *454*, 51-1–15-13, 1989.

Shettle, E. P., and R. W. Fenn, Models for the aerosols of the lower atmosphere and effects of humidity variations on their optical properties, *Environ. Pap. No. 676*, Air Force Geophys. Lab., Boston, Mass., 1979.

Slaper, H., H. A. J. M. Reinen, M. Blumthaler, M. Huber, and F. Kuik, Comparing ground-level spectrally resolved solar UV measurements using various instruments: A technique resolving effects of wavelength shift and slit width, *Geophys. Res. Lett.*, *22*, 2721–2724, 1995.

Stamnes, K., S. C. Tsay, W. Wiscombe, and K. Jayaweera, A numerically stable algorithm for discrete-ordinate-method radiative transfer in multiple scattering and emitting layered media, *Appl. Opt.*, *27*, 2502–2509, 1988.

Swartz, W. H., Quantifying photolysis rates in the troposphere and stratosphere, Ph.D. thesis, U. of Maryland, College Park, 2002.

Swartz, W. H., S. A. Lloyd, T. L. Kusterer, D. E. Anderson, C. T. McElroy, and C. Midwinter, A sensitivity study of photolysis rate coefficients during POLARIS, *J. Geophys. Res.*, *104*, 26,725–26,735, 1999.

van de Hulst, H. C., *Multiple Light Scattering: Tables, Formulas, and Applications*, vols. 1 and 2, Academic, San Diego, Calif., 1980.

van Weele, et al., From model intercomparison toward benchmark UV spectra for six real atmospheric cases, *J. Geophys. Res.*, *105*, 4915–4925, 2000.

World Meteorological Organization (WMO), Atmospheric ozone, 1985, Global ozone research and monitoring project, *Rep. 16*, Geneva, Switzerland, 1985.

A. F. Bais, Laboratory of Atmospheric Physics, Aristotle University of Thessaloniki, GR-54006 Thessaloniki, Greece. (abais@auth.gr)

J. Barrick and J. Crawford, NASA Langley Research Center, Hampton, VA 23681, USA. (j.h.crawford@larc.nasa.gov)

J. G. Calvert, C. A. Cantrell, G. D. Edwards, S. R. Hall, B. L. Lefer, S. Madronich, G. Pfister, and R. E. Shetter, Atmospheric Chemistry Division, National Center for Atmospheric Research, Boulder, CO 80303, USA. (calvert@acd.ucar.edu; cantrell@ncar.ucar.edu; gde@acd.ucar.edu; halls@ucar.edu; sasha@acd.ucar.edu; pfister@ucar.edu)

D. Flittner, Institute of Atmospheric Physics, University of Arizona, Tucson, AZ 85721, USA. (flittner@air.atmo.arizona.edu)

G. Frost, Aeronomy Laboratory, National Oceanic and Atmospheric Administration, Boulder, CO 80303, USA. (gfrost@al.noaa.gov)

B. G. Gardiner, British Antarctic Survey, Cambridge, CB3 0ET UK. (brian.gardiner@bas.ac.uk)

E. Griffioen, Department of Earth and Atmospheric Sciences, York University, Downsview, Ontario, Canada M3J 1P3. (erik@nimbus.yorku.ca)

A. Hofzumahaus and E.-P. Roeth, Institut für Chemie und Dynamik der Geosphäre Institut II: Troposphäre, Forschungszentrum Jülich, D-52425 Jülich, Germany. (a.hofzumahaus@fz-juelich.de; e.p.roeth@fz-juelich.de)

P. Johnston and R. McKenzie, National Institute of Water and Atmospheric Research, 50061 Lauder, New Zealand. (p.johnston@niwa.co.nz; r.mckenzie@niwa.co.nz)

P. Koepke, A. Ruggaber, and H. Schwander, Meteorological Institute, University of Munich, D-80333 Munich, Germany. (peter.koepke@lrz.uni-muenchen.de)

A. Kraus, Research and Development, Grünenthal GmbH, D-52099 Aachen, Germany.

M. Krol, Institute for Marine and Atmospheric Research, NL-3508TA Utrecht, Netherlands. (krol@phys.uu.nl)

N. Krotkov, Goddard Earth Sciences and Technology Center, University of Maryland at Baltimore County, Baltimore, MD 21250, USA. (krotkov@chescat.gsfc.nasa.gov)

A. Kylling, Norwegian Institute for Air Research, N-2027 Kjeller, Norway. (arve.kylling@nilu.no)

J. Lenoble, Equipe Interactions Rayonnement Solaire Atmosphere, Universite Joseph Fourier, F-38000 Grenoble, France. (jacqueline.lenoble@ujf-grenoble.fr)

S. Lloyd and W. H. Swartz, Applied Physics Laboratory, Johns Hopkins University, Laurel, MD 20723-6099, USA. (Steven.Lloyd@jhuapl.edu; bill.swartz@jhuapl.edu)

T. J. Martin, Karl-Franzens University, A-8010 Graz, Austria. (timothy.martin@gmx.de)

B. Mayer, Deutsches Zentrum für Luft-und Raumfahrt (DLR), D-82234 Wessling, Germany. (bernhard.mayer@dlr.de)

P. S. Monks, Department of Chemistry, Leicester, Leicester LE1 7RH, UK. (p.s.monks@le.ac.uk)

M. Mueller, Dresdener Bank AG, Jurgen-Ponto-Platz 1, D-60301 Frankfurt am Main, Germany. (JO1@gmx.net)

R. Schmitt, Meteorologie Consult GmbH, Auf der Platt 47, D-61479 Glashütten, Germany. (metcon@metcon-us.com)

M. van Weele, Royal Netherlands Meteorological Institute, NL-3730AE, DeBilt, Netherlands. (weelevm@knmi.nl)